UNIVERSITÀ DEGLI STUDI DI PADOVA

Dipartimento di Biologia

Corso di Laurea Magistrale in Biologia Evoluzionistica

TESI DI LAUREA

NLRP3 inflammasome activation in primary murine microglia and monocyte-derived human microglia

Laureando
Thomas Baratta

Relatore
Prof. Elisa Greggio
Dipartimento di Biologia

Correlatore
Prof. Olga Corti
Paris Brain Institute (ICM)

Anno Accademico 2022/2023

Index

1. Introduction

1.1 Microglia

Microglia are the resident immune cells in the central nervous system (CNS), playing a pivotal role in immune surveillance and maintenance of CNS homeostasis. Microglia represent the most abundant mononuclear phagocytes in the CNS, accounting for approximately 10% of cells and serving as brain macrophages: they are responsible for the elimination of microbes, dead cells, redundant synapses, protein aggregates, and other particulate and soluble antigens that may endanger the CNS [Saijo et al., 2011]. However, due to their unique homeostatic phenotype and their tight regulation by their specific microenvironment, they are distinct from other tissues macrophages [Paolicelli et al., 2022].

1.1.1 Microglial states and heterogeneity

Microglia display a high variability in its epigenome, transcriptome, proteome and metabolome, resulting in discrete morphological, ultrastructural and functional outputs (see Figure 1) [Paolicelli et al., 2022]. Such a variability depends on some intrinsic determinants (species, sex, ontogeny and genetic background), as well as on the specific context in which microglia is located. Particularly, sex-specific and region-specific transcriptional differences have been found in mouse microglia [Gunevkava et al., 2018; Villa et al., 2018]. For example, while cerebellar microglia show a more robust phagocytic transcriptional profile, striatal microglia show a weak phagocytic profile in the homeostatic state.

In addition, some studies in zebrafish and mouse models revealed that rapid changes occur in the microglial transcriptome during maturation, with developing microglia showing more heterogeneity than adult microglia [Mazzolini et al., 2020; Hammond et al., 2019; Li et al., 2019].

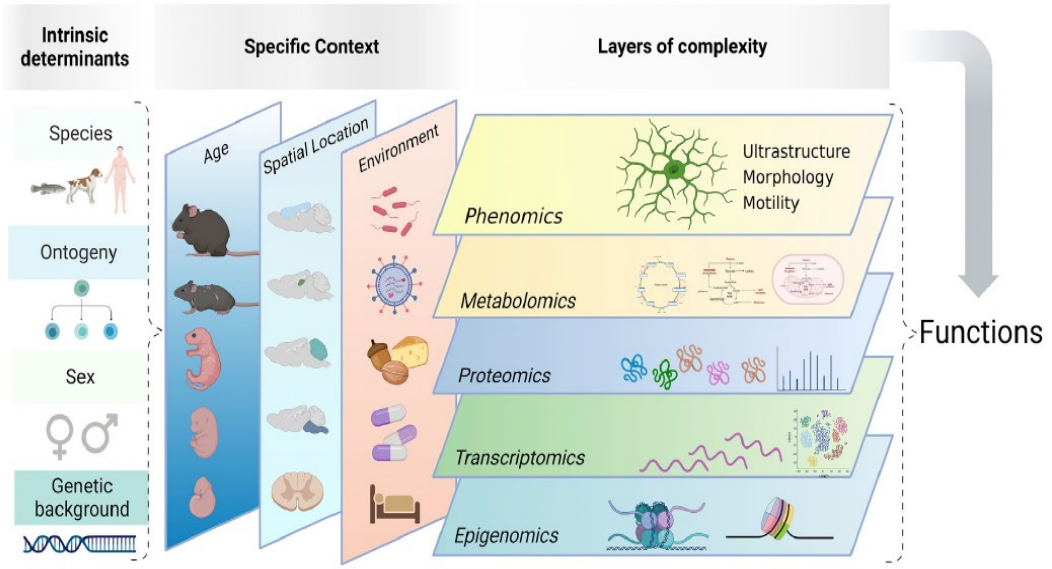

***Figure 1**: Microglial states depend on intrinsic determinants (such as species, ontogeny, sex, or genetic background) as well as the specific context they inhabit [RC. Paolicelli et al., 2022].*

Generally, "resting" microglia (i.e., microglia in a non-activated surveilling state) exhibit a highly ramified morphology with numerous branched processes [Paolicelli et al., 2022]. These processes extend and retract, enabling microglia to continuously monitor their local microenvironment. Such cells also display a low level of immunoreactivity and minimal production of pro-inflammatory cytokines or chemokines. However, as mentioned above, microglia are anything but static, as they are exceptionally responsive to alterations in their environmental context.

Microglia express many of the pattern-recognition receptors (PRRs) that sense pathogen-associated molecular patterns (PAMPs), including Toll-like receptors (TLRs) and NOD-like receptors (NLRs) [Saijo & Glass, 2011].

TLRs are localized to the plasma membrane or to the membrane of endocytic compartments. Following recognition of PAMPs, TLRs activate downstream signalling cascades, leading to the activation of nuclear factor-kB (NF-kB) and mitogen-activated protein kinase (MAPK) pathways, which eventually induce the transcription of pro-inflammatory mediators. In addition to mediating responses to PAMPs, TLRs also recognize endogenous damage-associated molecular patterns (DAMPs), induced by metabolic products and molecules released by dead cells [Saijo & Glass, 2011].

On the other hand, NLRs are a large family of cytoplasmic sensors that detect various foreign PAMPs and endogenous DAMPs. Some NLRs form multiprotein complexes termed inflammasomes (e.g., the NLRP3 inflammasome; see 1.4.2). Activation of inflammasomes leads to the maturation of pro-inflammatory mediators, such as interleukin-1β (IL1β), which initiate innate and adaptive immune responses in the cells [Saijo & Glass, 2011].

Consequently, upon any detection of signs for brain lesions or nervous system dysfunction, microglial cells undergo morphological and functional changes: "microglia activation" includes proliferation, migration to the site of injury and

release of several substances, such as pro-inflammatory cytokines [Kettenmann et al., 2011]. Pro-inflammatory cytokines released by PRR-mediated signaling, including IL1β and tumor necrosis factor α (TNFα), stimulate both innate and adaptive immunity by inducing the differentiation of effector T cells [Saijo & Glass, 2011].

Classically, microglial phenotypes have been divided into three main categories based on their activation: homeostatic state, pro-inflammatory state (M1 phenotype) and anti-inflammatory state (M2 phenotype). Each of these activation states is characterized by a distinct morphology, physiology and transcriptome, releasing different factors and serving different functions inside the CNS. However, such a traditional nomenclature is nowadays thought to be inadequate to accurately reflect the complexity of microglial activation [Paolicelli et al., 2022].

1.1.2 Ontogeny of microglia

The embryonic origin of microglia has been debated for a long time. Today there is consensus that microglial cells do not stem from the neuroectoderm, but rather derive from mesodermal progenitors [Kettenmann et al., 2011]. Fate mapping analysis established that microglia originate from primitive myeloid progenitors in the yolk sac, which migrate into the CNS during later development, whereas postnatal hematopoietic progenitors (in contrast with what occurs for most tissue macrophages) do not significantly contribute to microglia homeostasis in the adult brain [Ginhoux et al., 2010].

Therefore, microglia represent an ontogenically distinct population in the mononuclear phagocyte system; this evidence has implications for the use of monocyte-derived microglia-like cells (MDMis) in experimental essays (see 1.1.4).

1.1.3 Evolution of microglia

Microglia are classically considered to represent an evolutionary novelty, being exclusively present in vertebrates. If this is true in the strict sense, some old studies suggested the existence of a distinctive class of neuroglial cells comparable to vertebrate microglia in insects and mollusks [Sonetti et al., 1994], such as in the medicinal leech *Hiruda medicinalis* [Rio-Hortega, 1920]. Such microglia-like cells appear to resemble vertebrate microglia both morphologically in terms of their ramified processes, as well as in terms of phagocytic capacity. Furthermore, the two cell types have certain biochemical features in common, like the presence of certain cytokines [Sonetti et al., 1994], IBA1 protein expression, purinergic and NO-dependent responses [Sharma et al., 2021]. This evidence

would indicate that core features of microglial identity and function were present early in microglia and have been preserved through evolution. Future work would be needed to clarify the extent of divergence between vertebrate microglia and invertebrate microglia-like cells.

Regarding vertebrates, even though microglia are present in all the species, most of the studies are from rodents. However, some comparative studies have been conducted in order to assess microglia conservation across evolution. Geirsdottir et al. (2019) focused on 18 evolutionarily distant species, including *Hiruda medicinalis* as an outgroup. They observed a considerable range in terms of ramifications number, dendrite length and cell size between species (see Figure 2).

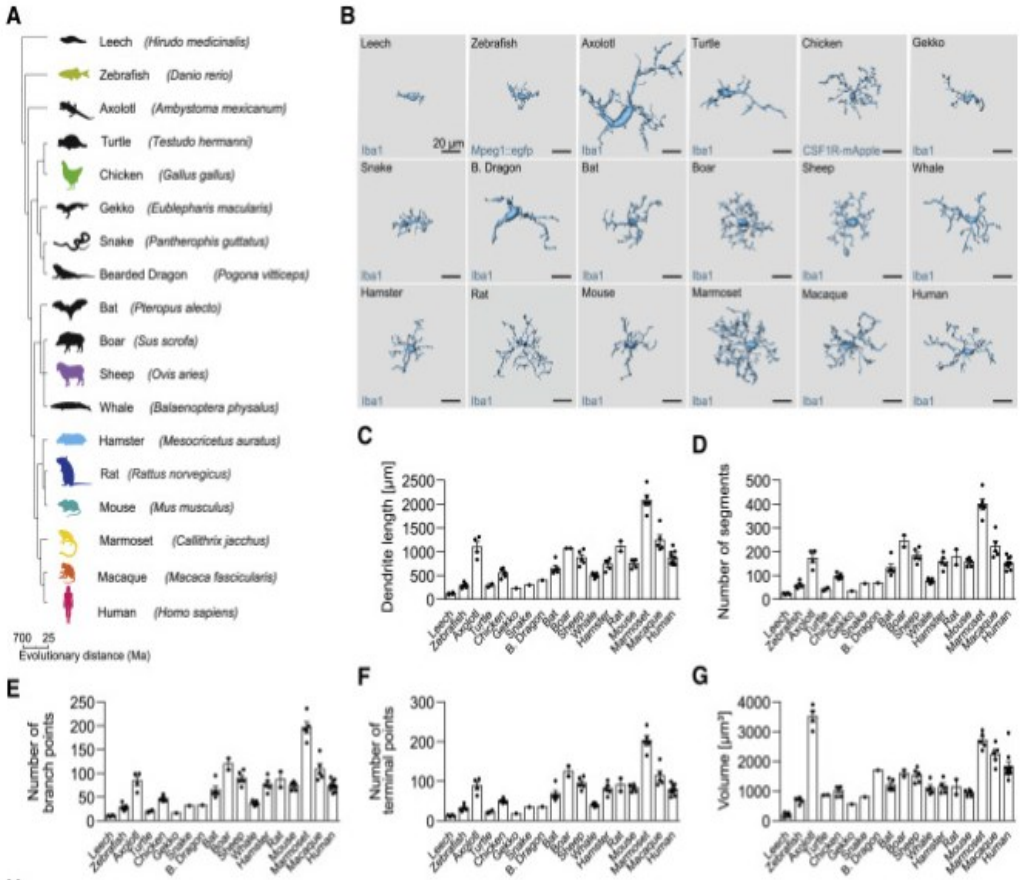

***Figure 2**: Morphological variability of microglia observed by Geirsdottir et al. (2019).*

A) Phylogenetic tree based on the NCBI taxonomy of animals used in this study. B) 3D reconstruction. (C-G) Cell morphometry of microglia. [Geirsdottir et al., 2019]

Further transcriptomic analysis revealed that microglia express a large set of conserved core genes across all mammalian species (and to a lower extent, even in zebrafish and chicken). These genes include transcription factors (*Spi1* and *Irf8*), lysosomal hydrolases (e.g., *Cst3*, *Ctsa*, *Ctss*, *Ctsb*, *Ctsh*, *Ctsc*, *Ctsz*, and *Hexa*) and genes previously linked to the homeostatic gene signature of microglia (*C1qc*, *P2ry12*, and *Tardbp*).

Such a relative homogeneity of microglia across vertebrates finds support in other transcriptional studies. As an example, adult zebrafish microglia, similar to their mouse counterparts, express Toll-like receptors, chemokine receptors, purinergic receptors, MHC class II, and complement receptor genes as part of their core microglial transcriptional repertoire [Oosterhof et al., 2017]. These findings indicate that the developmental, homeostatic, and physiological functions of microglia governed by these genes are conserved in early vertebrates.

However, to a higher magnification, mammalian microglia may be divided into two different clusters based on transcriptomic data (Figure 3): macaque showed the highest similarity to human microglia in terms of expression patterns, whereas laboratory mouse strains clustered together with wild mice and hamster [Geirsdottir et al., 2019]. For example, analysis of pathways specific to humans, macaques, marmosets and sheeps, revealed notable enrichment in DNA repair pathways when compared to rodents. These pathways have previously been associated with longevity [Ungvari et al., 2008].

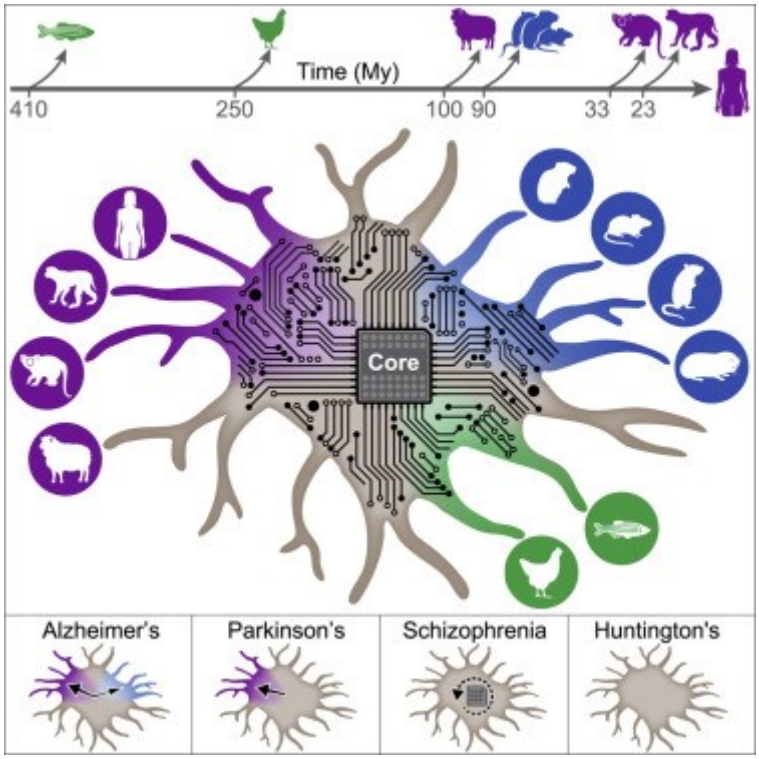

Figure 3*: Based on transcriptomic data, vertebrate species can be clustered into three groups. The human-specific cluster expresses more genes related to Alzheimer's and Parkinson's disease. [Geirsdottir et al., 2019]*

What is even more interesting in this context is that, among the genes whose expression is enriched in the human-specific cluster, several correspond to Alzheimer's and Parkinson's disease susceptibility genes (Figure 3). More specifically, enriched pathways include phagocytosis, autophagy, apoptotic cell clearance and ferroptosis [Geirsdottir et al., 2019].

Finally, single-cell transcriptomic analysis identified vast microglial heterogeneity in humans, in contrast to all other mammals, which mostly appear to display a single microglial type at steady state, under non-pathological conditions. Different subtypes were observed in both male and female microglia, unrelated to sex differences. These results suggest accelerated changes in microglia over the course of human evolution when compared to other non-human vertebrates.

Surprisingly, and probing the aforementioned heterogeneity, all tested human individuals (differently from mouse) presented a sub-population with increased expression of several inflammatory genes that have been linked with a senescence-associated secretory phenotype (SASP) [Geirsdottir et al., 2019]. This sub-population of microglial cells is known to be implicated in sterile inflammation, wound healing and age-related processes, including neurodegeneration [Bussian et al., 2018].

These findings not only suggest that microglial evolution has made *Homo sapiens* to some extent more prone to develop neurodegenerative disorders, but they also highlight how successful translation from neurodegenerative animal models to human clinical trials is far from adequate.

1.1.4 Monocyte-derived microglia-like (MDMi) cells

The growing appreciation that microglia have crucial roles in brain function in health and disease has led to an increasing interest in studying microglia in detail with more relevant models.

Because of the ethical and technical difficulties associated with access to human brain microglia, mouse models have predominantly been used to study microglia phenotypes and function thus far [Sargeant & Fourrier, 2022]. However, considering the high heterogeneity and variability of microglia, especially between mouse and human on a phylogenetic base (see 1.1.3), a validation in human models is needed to support the translational value of any result obtained in mouse.

The use of primary microglia obtained from deceased patients is comprehensibly limited by their availability and number.
As a consequence, the use of induced pluripotent stem cells (iPSCs) has been recently considered a more relevant approach to study human microglia, especially as it allows comparison of iPSC-derived microglia from healthy controls and patients with immune-related diseases, while maintaining an individual's genetic background [Sargeant & Fourrier, 2022]. However, such a model remains limited by scaling and time constraints (most protocols required over five weeks for the cells to differentiate into microglia) [Sargeant & Fourrier, 2022].

In this context, *in vitro* models of monocyte-derived microglia-like (MDMi) cells have been developed and characterized.

Banerjee et al. (2021) established that MDMi cells develop typical microglial ramified morphology, express microglial specific surface markers (P2RY12 and TMEM119) and possess phagocytic activity. This highlights the utility of this model in the study of microglial function in many brain diseases, such as Parkinson's disease.

As MDMi cells are derived from a simple blood sample, and their differentiation process takes no more than 10-14 days [Sargeant & Fourrier, 2022], this model allows to quickly and easily explore microglial function and phenotype.
Furthermore, RNA-seq data evidenced that MDMi cells show a transcriptomic signature which resembles human microglia more than animal models and immortalized microglia cell lines do [Ryan et al., 2017; Gosselin et al., 2017].

On the other hand, MDMi models are limited by the lack of three-dimensional spatial arrangement and interaction with other relevant brain cell populations (e.g. neurons, astrocytes) [Sargeant & Fourrier, 2022].
Moreover, contrary to iPSC-derived models (which generate hematopoietic microglial progenitors), the generation protocols do not mimic the ontogeny of microglia (see 1.1.2). Indeed, as MDMi cells are derived from monocytes, they are not actual microglia but surrogates that can represent important characteristics of human microglia [Sargeant & Fourrier, 2022].
Therefore, MDMi models are primarily useful for rapid screening studies, whose results could be validated using iPSC-derived microglia models and complex co-culture and 3D systems.

Finally, the lack of a standardized protocol to derive monocytes into microglia-like cells is currently a limitation to the use of MDMi [Sargeant & Fourrier, 2022]. Indeed, cells in culture are not only extremely sensitive to microenvironment, but there might be subject-to-subject variation regarding cell viability during the differentiation process. Ryan et al. (2017) showed that for 10% of individuals monocytes did not survive the differentiation process, although the reasons remain unknown. No other studies report this finding, which might be due to a lack of a standardized protocol.
This, however, means that the quality of differentiation must be validated individually.

1.2 Parkinson’s disease

Parkinson's disease (PD) is a chronic and progressive neurodegenerative disorder affecting mainly the CNS, which is characterized by the selective loss of dopaminergic neurons in the substantia nigra pars compacta (SNpc) in the midbrain, resulting in a decrease in the levels of dopamine in the basal ganglia.
It is the second most common neurodegenerative disorder after Alzheimer's disease (AD) [Bloem et al., 2021], affecting approximately 1% of individuals over the age of 60, with increasing prevalence in older age groups [Poewe et al., 2017].

1.2.1 History of PD

PD has a long and complex history dating back to ancient times.

The clinical syndrome of parkinsonism was known – and methodically treated - in ancient India, under the name of “Kampavata”, even before the period of Christ. The earliest reference to bradykinesia dates to 600 bc [Ovallath & Deepa, 2013].

Also, recorded descriptions of PD-like conditions date back to European ancient civilizations such as the Greeks and Romans. Hippocrates, for example, wrote about a condition he called "kamnos", characterized by tremors and rigidity. It has been suggested that the term "kamnos" was a reference to a type of barley that was used to make bread in ancient Greece, and that it was used as a metaphor for the tremors and stiffness associated with the condition [Berrios & Landau, 2016].

Similarly, Galen, a physician in the Roman Empire, described a condition known as "tremor universalis" (it's possible to read about such a condition in his work "De locis affectis").

However, while it is always interesting to look back at the historical roots, it is important to note that Hippocrates' and Galen's descriptions predate the modern medical understanding, and it is not clear whether their observations were related to the same condition that is currently known as PD.

It was not until the early 19th century that PD began to be recognized as a distinct clinical entity. The first detailed description of the disease was provided by James Parkinson in his monograph "An Essay on the Shaking Palsy," which was published in 1817 [Parkinson, 2002]. In this essay, Parkinson described six cases of individuals with what he called "paralysis agitans", characterized by a combination of tremors, rigidity, and bradykinesia.
The term "Parkinson's disease" was not coined until the late 19th century, when Jean-Martin Charcot, a French neurologist, began to use the term to describe the condition [Lees et al., 2009]. Charcot made significant contributions to the understanding of PD, particularly in the area of clinical diagnosis and classification.

In the early 20th century, the advent of new technologies, such as the electroencephalogram (EEG), helped to further advance our understanding of the disease [Bhidayasiri et al., 2013]. However, it was not until the 1960s that the discovery of dopamine (DA) as a neurotransmitter in the basal ganglia provided a

breakthrough in our understanding of the pathophysiology of PD [Lees et al., 2009].

In recent years, significant progress has been made in the identification of genetic risk factors for PD (see 1.5.3), as well as in the development of new therapies (see 1.6) such as deep brain stimulation and gene therapy [Fearnley & Lees, 2019].

Nonetheless, much remains to be learned about its underlying causes and the range of non-motor symptoms that are associated with PD.

1.2.2 Symptoms and diagnosis

Basal ganglia, and in particular the striatum, are fundamental structures involved in the control of voluntary movements, both by facilitating wanted movements and suppressing involuntary ones. DA is a key neurotransmitter released by this nervous circuitry for motor output control.

Therefore, DA depletion in the basal ganglia results in the hallmark motor symptoms of PD, including tremors - which are often the first symptom to appear -, rigidity, bradykinesia and postural instability [Dorsey et al., 2018]. It is noteworthy that by the time motor symptoms manifest, more than 50% of dopaminergic cells in the SNpc have already degenerated and striatal DA levels have decreased by 80%.

In addition to these motor symptoms, PD is also characterized by a range of non-motor symptoms, including cognitive impairment, autonomic dysfunction, depression, anxiety and sleep disturbances [Fan et al., 2021].

PD clinical manifestation is typically preceded by a long prodromal phase, which can last up to 20 years before the onset of motor symptoms. It is also associated with a range of non-specific symptoms such as olfactory dysfunction – anosmia -, mood disorders, constipation and REM sleep behavior disorder [Jewell et al., 2022].

The disease progression causes cognitive decline and dementia for most of the patients after 10 years from the diagnosis [Fan et al, 2021].

A definitive diagnosis for PD is normally possible through a post-mortem examination only. This is true, apart from few familial cases, which can be diagnosed thanks to genetic analysis.

Diagnosis for PD is usually based on clinical criteria, with the use of various diagnostic criteria, including the United Kingdom Parkinson's Disease Society Brain Bank Clinical Diagnostic Criteria and the Movement Disorder Society Criteria for Diagnosis of Parkinson's Disease. The diagnosis typically relies on the presence of at least two of the four primary motor symptoms (tremor, rigidity, bradykinesia, and postural instability), as well as the absence of atypical features [Bloem et al., 2021].

However, accurate diagnosis can be challenging, particularly in the early stages of the disease, when motor symptoms may be mild or non-specific.

1.2.3 Diffusion

Several studies have highlighted the increasing prevalence and incidence of PD globally, indicating that the disease is becoming a significant public health issue [Dorsey, Sherer & Okun, 2018; Poewe et al., 2017].

The exact number of people affected by PD worldwide is difficult to determine due to variations in diagnostic criteria and reporting. However, according to Bloem, Okun & Klein (2021), it is estimated that approximately 6.1 million people worldwide had PD in 2016, and this number is expected to double by 2040 [Dorsey, Sherer & Okun, 2018].

PD is more prevalent in developed countries, particularly in urban areas, suggesting that urbanization and industrialization may contribute to the diffusion of the disease [Dorsey et al., 2018]. In high-income countries, the prevalence of PD is projected to increase from 4.1 million cases in 2005 to 8.7 million cases by 2030 [Ascherio & Schwarzschild, 2016].

Such a trend is largely attributed to aging populations, urbanization and environmental factors, together with genetic predisposition [Checkoway et al., 1999]. Notably, PD is most commonly diagnosed in individuals over the age of 60, meaning that the prevalence of the disease increases with age [Lees, Hardy & Revesz, 2009].

1.3 Molecular pathogenesis of PD

As pointed out above, the neuronal loss in the SNpc is undoubtedly the principal pathological marker of PD. However, the neurodegenerative process is generally more widespread and slowly progressing, reaching – though to a lesser extent - other regions of the brain and therefore affecting non-dopaminergic neurons as well [D.W. Dickson, 2012].

The underlying molecular pathogenesis remains poorly understood and is suspected to involve multiple pathways and mechanisms: impaired α-synuclein proteostasis, mitochondrial dysfunction and oxidative stress, Ca^{2+} and metal dyshomeostasis, defects in axonal transport and neuroinflammation [Poewe et al., 2017] (see 1.4).

1.3.1 α-synuclein aggregates

α-Synuclein pathology is not exclusive for PD: an entire family of diseases shares such a particular characteristic. Dementia with Lewy Bodies (DLB), Multiple System Atrophy (MSA) and AD are other examples of synucleynopathies.

α -Synuclein is a small acidic protein consisting of 140 amino acids, which is encoded by the *SNCA* gene and primarily expressed in the presynaptical terminals within the central nervous system [Goedert, 2001].

α -Synuclein contains three domains (see Figure 4): an N-terminal domain (residues 1-60), a central domain (residues 61-95), and a C-terminal domain (residues 96-140) [Emin et al., 2022]. The N-terminal domain contains a highly conserved amphipathic α -helix and is responsible for the ability of the protein to interact with lipid membranes, a property that is essential for its physiological functions [Corti et al., 2011]. The central domain contains a highly conserved region, known as the non-amyloid- β component (NAC) region, which confers amyloidogenic properties to the protein and is critical for α -synuclein aggregation [Goedert, 2001]. The C-terminal domain is highly acidic and acts as a self-chaperone, counteracting the process of "amyloidogenesis", through which α-synuclein forms oligomers [Emin et al., 2022].

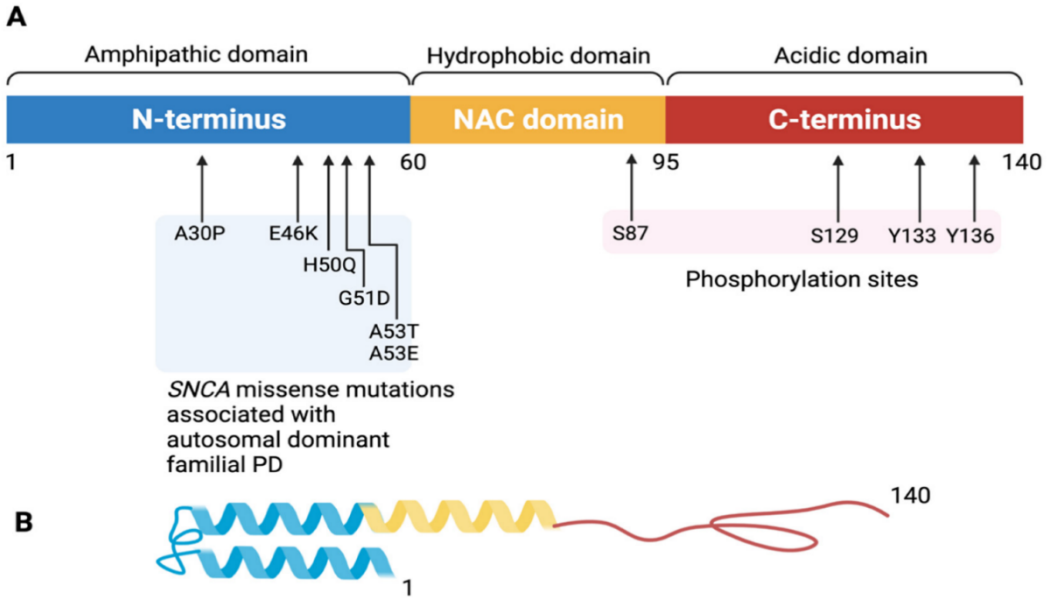

***Figure 4**: Structure of the alpha-synuclein monomer. (**A**) Schematic depiction of alpha-synuclein primary structure. (**B**) Tertiary structure of the α-synuclein monomer. [TS Fan et al., 202].*

The formation and diffusion of α-synuclein aggregates, named Lewy bodies (LBs) and Lewy neurites (LNs), is thought to be a key factor in the development and progression of PD [Corti et al., 2011], even though some of its forms do not manifest this particular feature (e.g., PRKN-related PD, see 1.5.3.2).

The heterogeneity of different co-existing aggregate species makes it hard to isolate and study their individual toxic properties.

Notably, Rochet et al. (2004) provided evidence that oligomeric intermediates of the α-synuclein fibrillization pathway, termed protofibrils, are neurotoxic. Moreover, DA reacts with α-synuclein to form a covalent adduct that slows the

conversion of protofibrils to fibrils, promoting the accumulation of toxic protofibrils [Rochet et al., 2004].

This might explain why DA neurons are most vulnerable to degeneration in PD.

Accordingly, Emin et al. (2022) recently suggested that small soluble α -synuclein aggregates, rather than fibrils or larger complexes, are the toxic species in PD.

1.3.2 Mitochondrial dysfunction

Mitochondrial dysfunction, together with the loss of DA neurons in the SNpc and the accumulation of α -synuclein aggregates, is a core aspect of PD pathophysiology [Shapira et al., 1990].

Due to their rich axonal arborization and pace-making activity, DA neurons in the SNpc have a high energy demand. An imbalance in turnover and function of mitochondria might impair cell homeostasis and finally lead to cell death.

Moreover, a dysfunction in the electron transport chain in mitochondria leads to an increase in the production of reactive oxygen species (ROS), consequently exacerbating oxidative stress. Oxidative stress, in turn, is intimately linked to several components of the degenerative process, contributing to the cascade leading to dopaminergic cell death in PD [P. Jenner, 2003].

Notably, Shapira et al. (1990) found, in a postmortem study, that complex I and NADH cytochrome *c* reductase activities were significantly reduced in the SN of PD patients, with respect to controls. In addition, they observed that the same specific defect of complex I is produced by the compound MPTP (1-methyl-4-phenyl-1,2,3,6-tetrahydro-pyridine), used to generate an animal model of PD, that is selectively toxic for DA-containing cells of the SN. This compound can pass the blood-brain barrier as a lipophilic compound; once inside the brain, it is converted into its active form (MPP+) by the mitochondrial monoamine oxidase B (MAO-B) in glial cells. MPP+ interferes with mitochondrial complex I and leads to the production of ROS, further exacerbating cellular damage [Jackson-Lewis & Smeyne, 2005].

The selective toxicity of MPP+ for DA neurons is linked to the capability of this compound to exploit the synaptic carriers for DA reuptake (DAT) [Jackson-Lewis & Smeyne, 2005].

A possible link between mitochondrial complex I activity and PD has been suggested based on these results. Moreover, an environmental toxin with action similar to that of MPTP might contribute to the development of PD [Shapira et al., 1990].

But mitochondria are not just energy producing organelles, fundamental for the sustenance of metabolic needs. They play an important role in modulating immune responses and neuroinflammation.

Finally, the products of some PD-related genes, such as PRKN (see 1.5.1.2) or DJ-1, are localized in mitochondria. Zhang et al. (2005) have demonstrated that DJ-1 interacts with and regulates the activity of multiple proteins involved in mitochondrial function and oxidative stress response, such as mitochondrial Complex I and peroxiredoxin 2.

1.4 Neuroinflammation

Neuroinflammation can be defined as the activation of the brain's innate immune system in response to an inflammatory challenge, such as infections, injuries or toxic insults. It is a complex physiological response involving the activation of immune cells, including microglia, astrocytes and infiltrating peripheral immune cells, and the consequent release of inflammatory mediators like cytokines, chemokines and ROS in the CNS. This process triggers an inflammatory cascade that results in cellular and molecular changes in the brain.

While neuroinflammation can be beneficial, such as in response to acute infections or injuries, chronic or excessive neuroinflammation can have detrimental effects on neuronal function. Inflammatory mediators can indeed promote excitotoxicity, oxidative stress and apoptosis, promoting neurodegeneration and cognitive impairment.

Neuroinflammation has been implicated in the pathogenesis of various neurological disorders, including AD and PD.

The existence of an autoimmune component in PD was strongly suggested in 1988 by McGeer et al., who tracked activated microglia, together with pro-inflammatory cytokines, in the SN of PD patients' post-mortem brains. Moreover, several of the 90 genetic risk variants associated with sporadic PD are found in immune-related genes [Bloem et al., 2021]. This evidence corroborates the hypothesis of an autoimmune component in PD.

1.4.1 Role of microglia in PD-linked neuroinflammation

As a result of their high sensibility to their local environment (see 1.1.1), microglia are the primary mediators of neuroinflammatory response which are notably thought to be a significant contributor in the progression of neurodegenerative disorders, such as PD.

Microglia-mediated neuroinflammation in PD is supported by studies showing the upregulation of various pro-inflammatory cytokines, such as TNFα, IL1β and interleukin-6 (IL6), in the CNS of PD patients [Kwon & Koh, 2020].

In PD, microglia have been shown to adopt an activated pro-inflammatory state characterized by increased expression of surface markers such as human

leukocyte antigen-DR (HLA-DR), which is indicative of their antigen-presenting capability [McGeer et al., 1988].

Emerging evidence suggest that microglia in PD undergo specific metabolic changes that further contribute to their pro-inflammatory phenotype. For instance, microglia have been shown to exhibit increased glycolytic metabolism, leading to increased production of lactate, which can further promote neuroinflammation by, in turn, activating microglia [Aldana, 2019]. Additionally, dysregulated lipid metabolism in microglia has been linked to the production of neurotoxic molecules such as ROS and prostaglandins, which can further exacerbate neuroinflammation and contribute to dopaminergic neuron loss in PD [Aldana, 2019].

Furthermore, microglia are involved in the phagocytosis of α -synuclein aggregates and participate in their degradation through various pathways, including autophagy and lysosomal pathways. These pathways are often impaired in chronic neuroinflammatory conditions [Kwon & Koh, 2020].

Finally, microglia closely communicate with astrocytes: they are also emerging to play an important role in neuroinflammatory processes and neurodegenerative diseases [Kwon & Koh, 2020].

1.4.2 NLRP3 Inflammasome

Neuroinflammation pathways are triggered and regulated by the action of inflammasomes, multiprotein complexes formed in the cytoplasm of cells upon the detection of pathogen-associated molecular patterns (PAMPs) or damage-associated molecular patterns (DAMPs). Precisely, inflammasomes regulate the activation of Caspase-1 (Casp-1), inducing inflammation through the processing and release of the pro-inflammatory cytokines IL-1β and IL-18. These cytokines can also initiate pyroptosis, a type of programmed cell death that is triggered by infection or cellular stress [Guo et al., 2016].

The general composition of inflammasomes contemplates the presence of a pattern recognition receptor (PRR) and procaspase-1, precursor of Casp-1; in most of cases, an adaptor protein is also required for procaspase-1 recruitment [Kelley et al., 2019].

Together with AIM2 and pyrin inflammasome, the most extensively studied inflammasomes are those belonging to the NOD-like receptors (NLR) family. Among them, several studies have demonstrated that the upregulation of the NLRP3 inflammasome is a key contributor to the progression of inflammatory and neurodegenerative diseases, including PD [Hulse & Bhaskar, 2022; Jewell et al., 2022].

Reflecting the general structure of inflammasomes, the NLRP3 inflammasome is made up of the NOD-like receptor protein 3 (NLRP3) and the apoptosis-associated speck-like protein (ASC), as well as procaspase-1 (Figure 5).

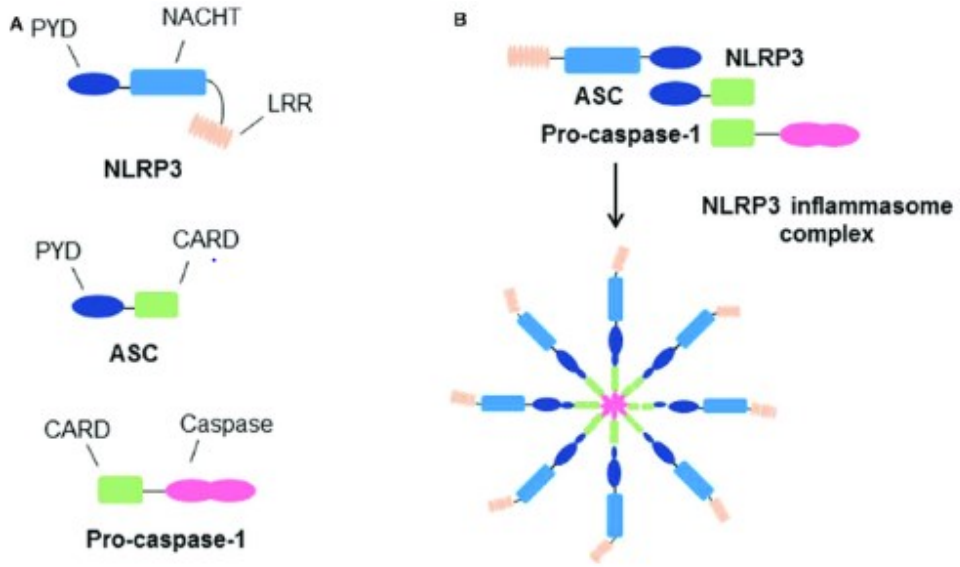

***Figure 5**: structure of NLRP3 protein (A) and NLRP3 inflammasome complex (B). Adapted from [S. Hamarsheh et al., 2020].*

NLRP3 protein is composed of several distinct domains, including an N-terminal pyrin domain (PYD), a central NACHT domain, and a C-terminal leucine-rich repeat (LRR) domain. The PYD domain of NLRP3 mediates the interaction with the adaptor protein ASC, which contains in turn a PYD and a caspase-recruitment domain, while NACHT domain, thanks to ATPase activity, is essential for inflammasome oligomerization. The function of LRR domain is not fully understood, but it is thought to be involved in ligand recognition and binding [Kelley et al., 2019].

Classical activation of the NLRP3 inflammasome follows a two-steps mechanism which comprises a priming and an activation step (Figure 6).

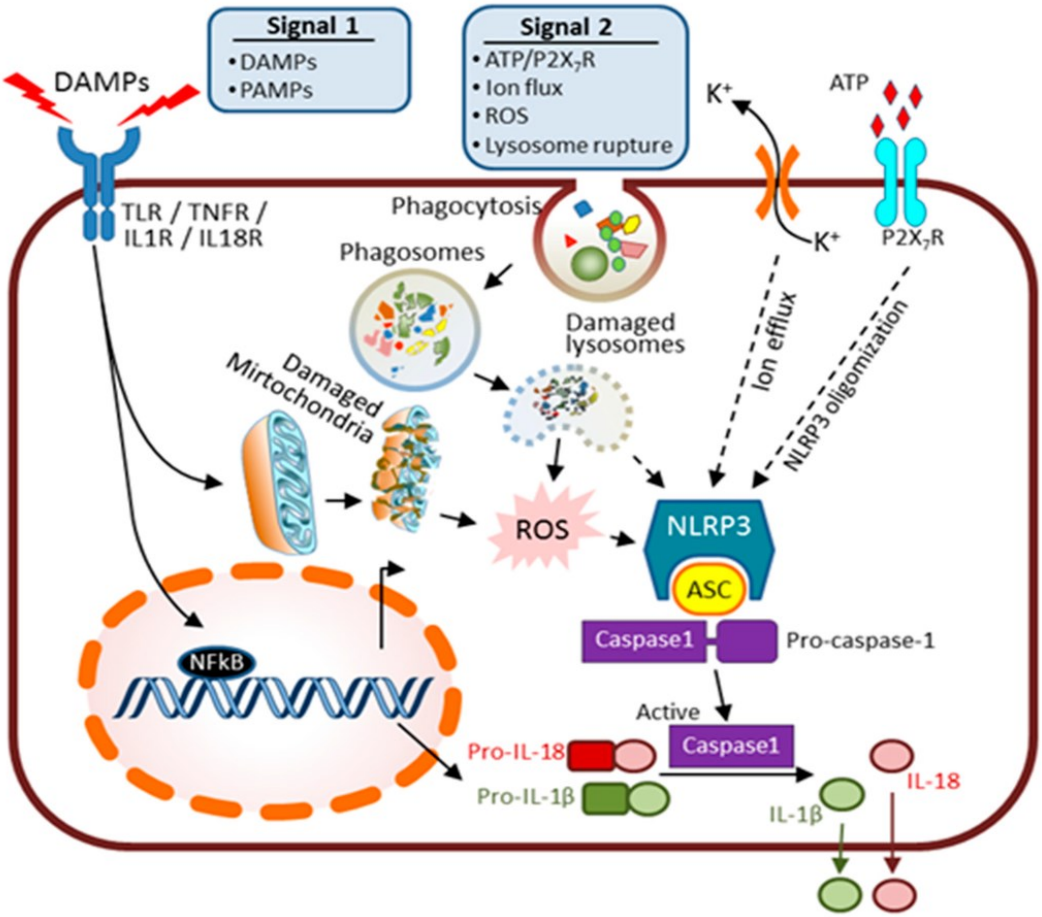

***Figure 6**: two-steps mechanism of NLRP3 inflammasome activation [Duann et al., 2016]*

The priming step involves the upregulation of NLRP3 and pro-IL-1β expression by the NF-κB (nuclear factor kappa-B, a pro-inflammatory transcription factor) pathway in response to various stimuli, such as PAMPs or DAMPs. This step also involves the induction of other pro-inflammatory cytokines, such as TNF-α and IL-6, which contribute to the inflammatory response [Zhong et al., 2016]. Priming is a necessary step, but it is not sufficient to support the function of the inflammasome. The second step, that is activation, involves the assembly of the NLRP3 inflammasome complex and the proximity-induced autocatalytic cleavage of pro-caspase-1 to form active Casp-1 (p20 fragment), which can then cleave pro-IL-1β and pro-IL-18 to form the active cytokines (IL-1 β and IL-18). This step can be triggered by a variety of stimuli, including extracellular ATP, crystals such as monosodium urate (MSU) or cholesterol crystals, and ROS generated by damaged mitochondria, as well as lysosome rupture [Zhou et al., 2011]. Preceding NLRP3 inflammasome assembly, ASC protein undergoes oligomerization, forming sizable specks (approximately 1 μm in diameter). This speck formation serves as an indicator of inflammasome assembly before Casp-1 activation and IL-1β processing. The exact mechanism driving NLRP3 activation downstream of these signals is still controversial, but K+ efflux seems to be the common

denominator for most of the above-mentioned stimuli [Muñoz-Planillo et al., 2013].

1.5 Etiology

PD is a complex disorder with multifactorial etiology, involving both genetic and environmental factors. While the exact causes of PD are not fully understood, a distinction can be made between monogenic and idiopathic forms.

Monogenic PD is caused by mutations in a single gene, while idiopathic PD is not linked to a specific mutation. Approximately 5-10% of PD cases are monogenic, with mutations in either one of more than fifteen identified genes, including SNCA, LRRK2 (see 1.5.1.1), and PRKN (see 1.5.1.2) being the most common [Bloem et al., 2021]. These mutations are typically inherited in an autosomal dominant or recessive manner and can result in early-onset PD.

Idiopathic PD, on the other hand, accounts for most of the cases (around 90%) and is believed to be caused by complex interactions between genetic susceptibility and environmental factors. Sporadic PD is the most common form of idiopathic PD and occurs in individuals with no family history of the disease.

As Elbaz et al. (2016) reported, the epidemiologic approach allowed to identify some protective and risk factors associated to the development of PD.

Among them, the most evident and intelligible risk factor is represented by aging, probably due to the accumulation of cellular damages over time, as the disease primarily affects older adults.

Exposure to environmental toxins, such as pesticides and heavy metals, has been linked to an increased risk of PD as well [Elbaz et al., 2016].

On the other hand, some existing meta-analysis reveal that caffeine consumption, smoking and physical activity are protecting factors against PD, each one being associated with ~30% reduction in the risk of developing the disease [Grosso et al., 2018; Hernan et al., 2002; Chen et al., 2005]. The exact mechanism by which they protect from PD are still unclear.

1.5.1 Genetic factors

It is becoming increasingly clear that genetic factors contribute to PD's complex pathogenesis. Rare forms of PD with a Mendelian inheritance are being investigated because of their importance to identify neurodegenerative mechanisms which may be shared between familial and sporadic PD, at least in some cases [Corti et al., 2011]. Over the past decades, through genetic studies in

families with high risk of PD recurrence, at least 23 disease-segregating genes or loci causing various monogenic forms of PD have been identified so far [Karimi-Moghadam et al., 2018].

Furthermore, genome-wide association studies (GWAS) provided additional risk loci which contribute to sporadic forms. 90 independent significant risk signals have been identified across 78 genomic regions, which would explain 16–36% of the heritable risk of PD [Nalls et al., 2019].

1.5.1.1 Leuchine-rich repeat kinase 2 (LRRK2)

Mutations in *LRRK2*, encoding the Leucine-Rich Repeat Kinase 2, are the most common cause of familial PD.

LRRK2 is a multidomain kinase belonging to the Ras of Complex (ROCO) protein superfamily, whose structure has been extensively studied to gain insights into its function and role in PD (Figure 9).

It is composed of 2527 amino acids and includes several protein-protein interaction domains together with a catalytic core.

The catalytic core of LRRK2 contains a Ras of complex (Roc) domain followed by a C-terminal of Roc (COR) domain. The Roc-COR domain tandem exhibits GTPase activity and is thought to regulate LRRK2 kinase activity. This region also serves as a scaffold for the interaction with other proteins involved in the same signaling pathways [Usmani et al., 2021].

The COR domain, furthermore, links ROC to the kinase domain, which is one of the most well-characterized regions of LRRK2. The kinase domain possesses ATP-binding and catalytic sites, enabling LRRK2 to phosphorylate various downstream substrates [Usmani et al., 2021].

Besides its two enzymatic domains, LRRK2 exhibits four protein-protein interaction regions [Usmani et al., 2021]. At the N-terminus, there is an armadillo repeat domain, which facilitates protein-protein interactions and may play a role in regulating LRRK2 cellular localization and binding partners. Downstream of the armadillo repeat domain is the ankyrin repeat domain, which is known to interact with 14-3-3 proteins through a phosphorylated cluster of serine residues. This interaction regulates LRRK2 stability and function.

The LRR domain, located between the ankyrin repeat and the Roc-COR domains, contributes to the overall three-dimensional structure of the protein and enables LRRK2 to interact with various binding partners.

The WD40 domain is located towards the C-terminal end of the protein and has been suggested to play a role in LRRK2 dimerization and subcellular localization.

The inactive protein is a monomer with a J-shaped conformation and the WD40 domain folding over the LRR domain, resulting in interaction between the LRR and kinase domains which prevents ATP binding and substrate access (Figure 7).

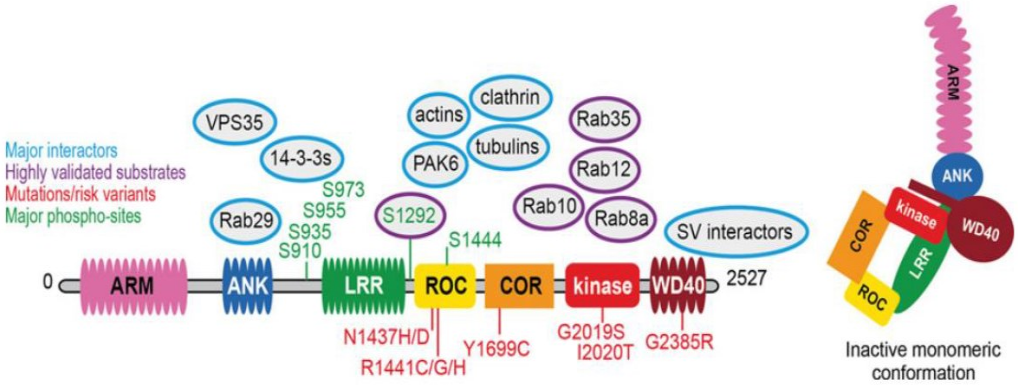

***Figure** 7: LRRK2 structure and inactive monomeric conformation [Iannotta & Greggio, 2021]*

On the other hand, the optimal enzymatic activity requires homodimerization through either the COR or the WD40 domain [Iannotta & Greggio, 2021].

The most well-characterized substrates of LRRK2 are members of the Rab family of GTPases: 10 Rabs expressed in human cells - Rab3a/b/c/d, Rab8a/b, Rab10, Rab12, Rab35, and Rab43 - seem to be endogenous substrates of LRRK2 [Pfeffer, 2022]. Rabs play a role in intracellular vesicular trafficking, and their activity is regulated by LRRK2-dependent phosphorylation in their switch II domain, which mediates GTP hydrolysis and the interaction with other regulatory proteins [Pfeffer, 2022].

LRRK2 expression is higher in peripheral tissues like kidneys, lung and peripheral immune cells than in the brain [Usmani et al., 2021]. However, in neuronal cells, *LRRK2* expression has been observed in both dopaminergic and non-dopaminergic neurons and is more pronounced in the putamen, region of the brain which receives afferences from the substantia nigra [Iannotta & Greggio, 2021]. *LRRK2* expression has also been reported in microglia [Russo et al., 2015] and other cell types, such as astrocytes and oligodendrocytes [Wallings & Tansey, 2019; Weindel et al., 2020].

The inactive form is bound and stabilized in the cytosol by the adaptor proteins 14-3-3 [Iannotta & Greggio, 2021]; following activation, LRRK2 disassociates from 14-3-3 and links to various membrane-bound compartments within cells. It has been detected in the endoplasmic reticulum (ER), Golgi apparatus, mitochondria, lysosomes, and synaptic vesicles [Usmani et al., 2021; Bonet-Ponce & Cookson, 2021].

Such a widespread localization suggests an involvement of LRRK2 in several pathways and functions, conferring to the enzyme its pleiotropic character. Indeed, LRRK2 has been implicated in multiple cellular processes.

Associated with the mitochondrial compartment, it is involved in mitochondrial fission and fusion dynamics, as well as in the maintenance of mitochondrial

homeostasis, and particularly the regulation of mitophagy [Ho et al., 2019]. In lysosomes, LRRK2 can act in a cell type-specific manner, regulating receptor recycling and autophagic flux in neurons and phagocytic and autophagic clearance in microglia [Cogo et al., 2020]. Furthermore, LRRK2 plays a role in the pre-synaptic compartment by modulating vesicle release and endocytosis [Bonet-Ponce & Cookson, 2021].

Finally, LRRK2 has been found to play a role in the regulation of immune responses, promoting pro-inflammatory reactions. Evidence about LRRK2 involvement in inflammatory pathways can be found with the identification of some genetic variants which make carriers more prone to develop inflammatory diseases like leprosy, Chron's disease and inflammatory bowel disease [Wallings et al., 2020].

What is more significant concerning PD, LRRK2 can also impact the activation and function of microglia.

Specifically, Russo et al. (2015) have demonstrated that following an NLRP3 activation paradigm, *LRRK2*-KO primary microglia exhibit a lower response than controls, displaying reduced levels of IL-1β mRNA and protein. Still, the precise molecular link with the NLRP3 inflammasome remains elusive. The same authors showed that LRRK2 positively regulates the activity of NF-κB.

Moreover, LRRK2 levels are upregulated upon LPS stimulation, in both human and murine microglia [Zhang et al., 2022].

So far, six PD-linked *LRRK2* mutations have been identified; all of them fall within the catalytic core of the protein and increase its enzymatic activity, both by enhancing its kinase activity or by decreasing the GTPase activity [Cogo et al., 2020]. Specifically, the Glycine-2019-serine (G2019S) mutation causes 10% of the familial PD cases, leading to a three-fold increase in kinase activity compared to the normal protein [Russo et al., 2015].

The exact mechanism by which *LRRK2* mutations participate in the neurodegenerative process associated with PD is not yet clear, but the pathogenic relevance of such a gene is strongly suggested by its implication in neuroinflammatory, mitochondrial and lysosomal pathways.

1.5.1.2 PRKN and PINK1

Mutations in two genes associated with mitochondrial function, *PINK1* and *PRKN*, represent the most common cause of juvenile familial PD, specifically those forms inherited in an autosomal recessive manner [Corti et al., 2011].

These two genes code respectively for PINK1 and Parkin, two widely expressed proteins essential for various processes associated with mitochondrial health and quality control, among which mitophagy is the best characterized. Some of these processes are associated with degradation of mitochondrial components, such as mitophagy itself and the formation of mitochondria-derived vesicles (MDVs), which facilitate the specific degradation of oxidized or damaged mitochondrial

content. Furthermore, PINK1 and Parkin are involved in regulating mitochondrial biogenesis. They contribute to the targeting and localized repression of mRNAs encoding specific respiratory chain subunits and promote the proteasomal degradation of the transcriptional repressor PGC-1α [Jin & Youle, 2012].

More in detail, PINK1, or PTEN-induced kinase 1, is a serine threonine kinase that acts as an upstream regulator of Parkin function.

In healthy mitochondria, it is imported into the inner mitochondrial membrane (IMM), where it is cleaved by specific proteases before being stored to the cytosol for degradation by the proteasome. Therefore, endogenous PINK1 levels are low under basal conditions. When sustained mitochondrial damage occurs, accompanied by reduced mitochondrial membrane potential, PINK1 fails to be imported into the IMM and accumulates on the outer mitochondrial membrane (OMM). Here, it phosphorylates ubiquitin molecules present on OMM proteins. Phosphorylated ubiquitin acts as a receptor for Parkin, attracting the protein to damaged mitochondria and triggering its activation through PINK1-dependent phosphorylation of its N-terminal ubiquitin-like domain [Narendra et al., 2010].

Parkin, a cytosolic E3 ubiquitin ligase, becomes activated upon recruitment to the OMM and initiates a cascade of polyubiquitination events targeted to numerous OMM proteins. The ubiquitin chains on the OMM then recruit autophagy receptors, leading to the engulfment of mitochondria into autophagosomes and their subsequent autophagic degradation, known as mitophagy [Jin & Youle, 2012] (Figure 8).

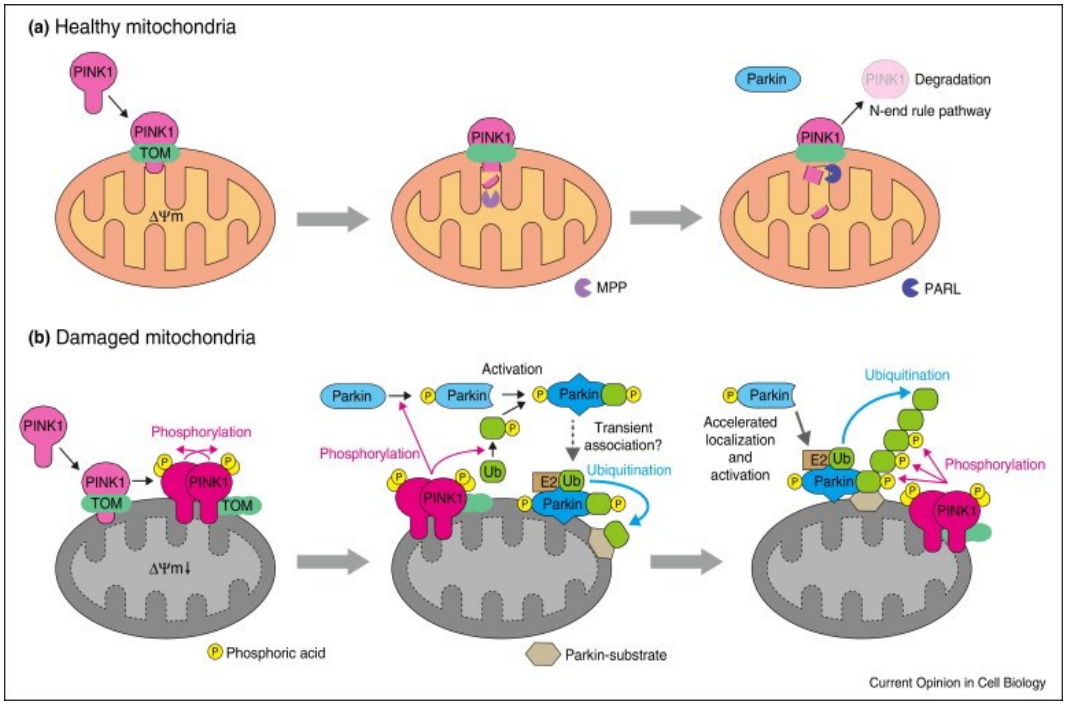

***Figure 8**: Schematic representation of the PINK1-Parkin mediated mitophagy [Eiyama & Okamoto, 2015]*

Mutations in *PRKN* and *PINK1* disrupt this mitochondrial quality control pathway, resulting in the accumulation of damaged mitochondria and subsequent

neuronal death, which supports the contribution of these mechanisms to the onset of PD [Pickrell et al., 2015].

Furthermore, Mouton-Liger et al. (2018) demonstrated that the activity of the NLRP3 inflammasome pathway is exacerbated in cultured Parkin-deficient mouse microglia and macrophages, as well as in human monocyte derived macrophages from patients with *PRKN* mutations. In particular, upon stimulation with lipopolysaccharide (LPS) and 3'-O-(4-Benzoylbenzoyl) ATP (BzATP), a higher release of the inflammasome-related cytokines IL1β and IL18 was detected in the absence of functional Parkin.

However, this field of research is relatively recent and the link between *PRKN* mutations, PD and chronic inflammation is still obscure.

1.6 Therapeutic approaches

At the moment, no therapy is available to prevent the onset of PD or arrest its progression. However, different therapeutic approaches are being tested, including pharmacological treatments, deep brain stimulation (DBS), stem cell-based therapies and gene therapy [Poewe et al., 2017].

The most common pharmacological treatment for PD consists in the use of levodopa (L-DOPA), the precursor of dopamine, in order to replenish dopamine levels in the brain [Poewe et al., 2017].

Currently, the most attractive molecular target to develop drugs against PD is LRRK2, whose kinase activity contributes to the pathogenesis of both familial and idiopathic forms of the disease [Atashrazm & Dzamko, 2022]. Indeed, patients with *LRRK2*-associated PD constitute a homogeneous subgroup with shared underlying pathophysiology [Tolosa et al., 2020].

Preclinical studies indicated that reduction of LRRK2 activity or expression is neuroprotective [Tolosa et al., 2020]; therefore, small-molecule LRRK2 inhibitors and antisense oligonucleotides have been developed and are now considered suitable for clinical exposure.

At present, two classes of LRRK2 inhibitors have been identified: type I and type II inhibitors, which interact with the active conformation of kinase and kinase inactive forms respectively. Type I inhibitors bind to the adenine region of ATP, while type II inhibitors interact with the ATP-binding site and its adjacent allosteric site, which only exists in the inactive conformation of the kinase [Hu et al., 2023].

DNL151, also known as BIIB122, is a selective and CNS-penetrant small molecule type I inhibitor of LRRK2. Like all type I inhibitors, BIIB122 acts by inducing dephosphorylation of Ser910 and Ser935 residues, as well as nearby sites [Hu et al., 2023].

In phase I and Ib clinical trials, BIIB122 was well tolerated with no serious adverse events [Jennings et al., 2023].

Furthermore, in both healthy volunteers and PD patients, well-tolerated doses of the drug resulted in median time-averaged reductions of approximately 85% in pS935-LRRK2 and pT73-Rab10 (one of the most common substrates of LRRK2 kinase), as well as a decrease in urine bis (monoacylglycerol) phosphate (BMP), which demonstrates the modulation of the lysosomal pathway downstream of LRRK2 [Jennings et al.,2023].

Based on these positive results, BIIB122 has recently been approved for phase III clinical trials [Hu et al., 2023].

2. Aims of the project

State-of-the-art breakthroughs in PD research indicate neuroinflammation as a candidate contributor to the progression of this neurodegenerative disorder. In particular, the up-regulation and activation of NLRP3 inflammasome have been found to play a role in the neurodegeneration occurring in PD (see 1.4). However, there is no clear report in literature about the possible link between the NLRP3 pathway and *LRRK2*, the gene causing most of PD familial cases (see 1.5.3.1).

Previous experiments conducted in the lab [L. Ballotto, unpublished data], revealed that mouse primary microglia carrying the *LRRK2*-G2019S mutation exhibit an upregulation of NLRP3 protein expression. In fact, NLRP3 protein is encoded by a target gene of NF-kB signalling, and it has been shown that *LRRK2* kinase positively regulates this specific pathway [Russo et al., 2015].
Striatal G2019S microglia showed a substantial decrease in intracellular K+ levels, which has not been detected in astrocytes and cortical microglia [Ballotto, unpublished data]. As K+ efflux is the main event upstream of NLRP3 inflammasome activation (see 1.4.2), all together these results suggest that the NLRP3 inflammasome activation is exacerbated (or dysregulated) in *LRRK2*-G2019S mutant microglia.

Investigating this potential connection might be important to better understand the molecular processes involved in neurodegeneration, and consequently to identify new possible therapeutic targets.

On the other hand, an overactivation of the NLRP3 inflammasome upon stimulation with LPS+BzATP has been well established in Parkin-deficient mouse microglia and macrophages, as well as human macrophages [Mouton-Liger et al., 2018] (see 1.5.1.2). This aspect needs to be further investigated, as no evidence of an interaction between Parkin and the NLRP3 inflammasome has been provided in human microglia. Moreover, it is not clear which step of the NLRP3 inflammasome activation is impaired in *PRKN*-mutant genotype, despite indications about the possible implication of the A20 protein, a negative regulator of the NF-kB and NLRP3 inflammasome pathway [Mouton-Liger et al., 2018].

ASC protein oligomerization represents an indicator of the assembly of the NLRP3 inflammasome, which occurs before Casp-1 activation and IL1β release (see 1.4.2).

The aims of the first part of this project, carried out in Padova (in the lab of Professor Elisa Greggio), were:

- to assess ASC protein oligomerization in mouse primary microglia carrying the *LRRK2*-G2019S mutation;
- to highlight putative region-specific differences between cortical and striatal microglia.

To support the translational value of any result obtained in animal models, a validation in human models is required. Accordingly, the second part of this

project, carried out in Paris (ICM-Brain Institute, in the lab of Professor Olga Corti) involved the use of human MDMis (see 1.1.4) as a model.
One of the major limitations in the use of MDMis is represented by the lack of a standardized protocol for their differentiation (see 1.1.4); consequently, the validation of an efficient protocol for generating microglia-like cells is to be considered a preliminary need.

Accordingly, the specific aims of this part of the study were:

- to validate a protocol for MDMis differentiation and activation;
- to assess NLRP3 inflammasome pathway activation in hMDMis, including those generated from mutant *LRRK2*-G2019S PD patients, evaluating consistency of observations across mouse and human models;
- to investigate differences in NLRP3 inflammasome activation in hMDMis from *PRKN*-mutant PD patients compared to controls, checking for putative alterations in ASC protein oligomerization.

3. Materials and methods

3.1 Mouse model

Already established mouse primary microglia cultures were used. Cultures were generated according to established protocols [Russo et al., 2015; Russo et al., 2018; Russo et al., 2019], optimized in the lab.

3.1.1 Cellular treatment

Cells had been seeded at a density of 250.000 cells/well on poly-L-lysine coated coverslips in a 24-well plate.
Microglia were treated with 20ng/ml lipopolysaccharide (LPS) in an FBS-free cell culture medium for 3.5h. Subsequently, nigericin was added to the medium to a final concentration of 10μM, and cells were incubated for an additional time of 30 minutes. Nigericin is a microbial toxin that forms pores in the membrane, causing K+ efflux and consequent NLRP3 inflammasome activation.
After stimulation, cells were washed once with PBS and fixed in 4% paraformaldehyde (PFA) before immunostaining. Incubation in PFA was performed for 20 minutes at RT.

3.1.2 Immunostaining and image analysis

After PFA fixation, cells were rinsed three times with PBS and permeabilized in PBS-0.1%Triton-x100 (20 minutes, RT). Three further PBS washes were performed before adding a blocking solution (made up of PBS-5%FBS) to each well: incubation took 1h at RT.
Primary anti-ASC antibody (Adipogen™, AL177) was diluted 1:100 in blocking solution, and cells were incubated O/N in a humified cold chamber at 4ºC.
The following day, coverslips were washed three times with PBS to eliminate any excess of primary antibodies. Subsequently, they were incubated at RT for 1h with suitable secondary antibody conjugated to a fluorophore (anti-rabbit Alexa Fluor™ 488 1:200), prepared in blocking solution. Following incubation, cells were rinsed again three times with PBS and treated with Hoechst 33258 (Invitrogen™), diluted 1:10000 in PBS, for 5 minutes to visualize cellular nuclei. Finally, the coverslips were mounted using Mowiol (Calbiochem™) and allowed to dry O/N at 4°C.
Image acquisition was carried out using a Leica™ DMI4000 epifluorescence microscope. In order to distinguish the shape and contour of cells, bright-field channel was exploited. Five images were captured at a 40X magnification from each experimental condition.
Quantification of cells positive for nuclear and cytosolic ASC specks was conducted using the ImageJ software with the assistance of the cell counter plugin. The measurements were subsequently normalized based on the number of nuclei.

3.2 Human model

3.2.1 Establishment of human Peripheral Blood Mononuclear Cells (hPBMCs) culture

For the validation of a protocol for hMDMis differentiation and stimulation, PBMCs from three different healthy subjects were used. These subjects were not affected by any chronic or acute inflammatory disease, and they did not suffer from any neurological disorder.
Blood samples were collected at the Clinical Investigation Centre (CIC; APHP: ICM); written and informed consent was obtained from all participating subjects.

For the second part of this project, involving the characterization of *LRRK2*- and *PRKN*-mutant cells, previously isolated and frozen PBMCs were used. PBMCs samples from the following PD-patients and matched-controls were included in the study:

ID	Birth date	Withdrawal date	Status	Sex	Mutant gene	Mutation	Onset of symptoms	Date of diagnosis
BMV02MOV0016	17/02/1963	23/05/2022	control	F	LRRK2	NA	NA	NA
NS0104739	01/02/1966	23/05/2022	patient	F	LRRK2	G2019S	2018	2019
BMV02MOV0020	03/08/1966	31/08/2022	control	M	LRRK2	NA	NA	NA
NS0104887	08/01/1968	31/08/2022	patient	M	LRRK2	G2019S	entre 2016 et 2018	2018
BMV02MOV0021	05/02/1967	01/09/2022	control	M	LRRK2	NA	NA	NA
NS0105046	09/12/1970	01/09/2022	patient	M	LRRK2	G2019S	2014	2016
BWV02MOV0022	01/10/1970	16/09/2022	control	M	LRRK2	NA	NA	NA
NS0105052	02/08/1970	01/10/2022	patient	M	LRRK2	G2019S	n.d.	n.d.
BMV02MOV0009	05/08/1971	23/02/2022	control	M	PRKN	NA	NA	NA
NS0104745	31/05/1974	23/02/2022	patient	M	PRKN	c.222_231del (double heterozygous)	01/07/1989	01/07/2000
BMV02MOV0018	01/08/1990	15/06/2022	control	F	PRKN	NA	NA	NA
NS0100530	06/10/1987	15/06/2022	patient	F	PRKN	c.827del (heterozygous)	15/07/1999	23/05/2016

3.2.1.1 PBMCs isolation

PBMCs were isolated from fresh blood through density gradient centrifugation based on an already established protocol [Sellgren et al., 2017]. Briefly, right after withdrawal, the blood was mixed with PBS (Dulbecco's DPBS; Gibco™, D8537). The blood-PBS dilution was then added to a 50ml falcon tube containing Ficoll (Sigma, Histopaque, 10771), a density gradient centrifugation medium for separation of mononuclear cells (1 volume Ficoll for 2 volumes blood). Mixing of phases was avoided (Figure 9, a).
C entrifugation was performed at 400g, RT, for 30 minutes, in order to separate the different blood components. After centrifugation, a buffy layer of PBMCs is situated between plasma and Ficoll (Figure 9, b).

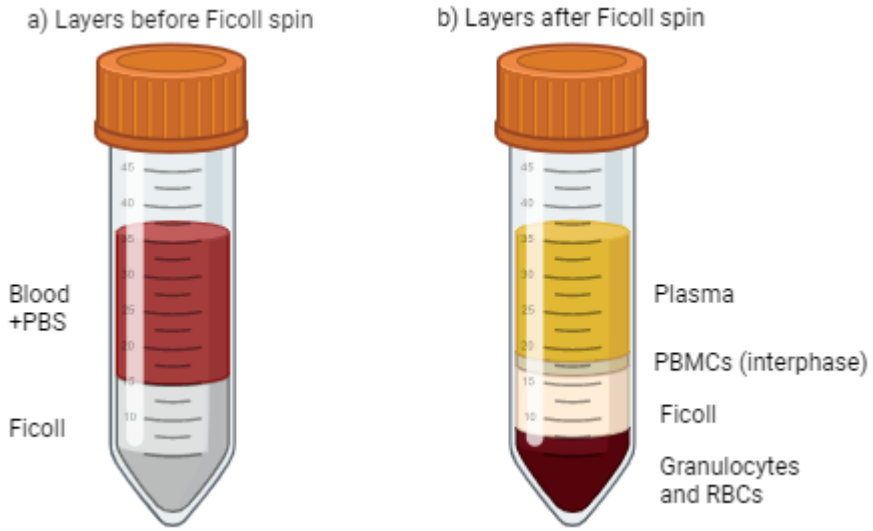

***Figure 9**: Layers before (a) and after centrifugation (b). a) Blood and Ficoll should not mix; b) The buffy coat containing PBMCs is between plasma and Ficoll.*

The buffy coat containing PBMCs was transferred in a fresh 50ml falcon tube and filled up with PBS. At least two cycles of centrifugation at 400g, RT, for 15 minutes, were performed to purify samples.

The cell pellet was resuspended in 1ml of RPMI (*Roswell Park Memorial Institute medium*) Glutamax 1640 (Gibco™, 61870044) enriched with 1% Penicillin/Streptomycin (P/S, GIBCO™, 15140122) and 10% heat-inactivated FBS (Gibco™, A3840401).

Cell number was counted using the automated cell counter ADAM™-MC.

3.2.1.2 PBMCs freezing and thawing

Isolated PBMCs were frozen in order to preserve them for subsequent experiments.
For freezing, the cell pellet obtained by centrifugation was resuspended in FBS supplemented with 10% dimethyl sulfoxide (DMSO, Sigma™, D8418)).
Each frozen vial contained ~$1*10^7$ PBMCs diluted in 1ml of FBS90%-DMSO10%. The vials were stored at -80ºC until usage.
Cryovials were thawed at 37ºC in a water bath. The cells were transferred to a 15ml falcon. 3ml of complete RPMI medium (RPMI Gmax 1640 with 1% P/S and 10% FBS) were added drop-by-drop, in order to minimize osmotic shock for optimized cell viability. The Falcon tubes were then filled up with 6ml of complete RPMI medium and centrifuged at 300g, RT, for 5 minutes.
The cell pellet was diluted in 1ml of complete RPMI medium and cell number was assessed using ADAM™-MC.

3.2.1.3 PBMCs seeding

PBMCs were diluted in an appropriate volume of complete RPMI medium, according to the desired density.
Cells were seeded onto 8-well chamber slides (ibidi™ 8 Well Chamber, 80826), previously coated with Geltrex (Thermofisher, A1413202).

Cell cultures were incubated at 37ºC, 5% CO_2.

3.2.1.4 Differentiation of hMDMis

The differentiation of PBMCs into microglia-like cells was promoted by adding the cytokines inter-leukine34 (IL34, R&D, 5265-IL-010/CF) and Granulocyte-macrophage colony-stimulating factor (gM-CSF, R&D, 215-GM-050/CF) to the culture medium, according to Sellgren et al. (2017).
In detail, the medium was changed the day after seeding to base RPMI medium (RPMI Gmax-1%P/S) enriched with 100ng/ml IL34 and 10ng/ml gM-CSF. Afterwards, a half medium change was performed every three days, meaning that half of the volume was aspirated from each well and substituted with a corresponding volume of Base RPMI Medium containing a double concentration of cytokines.
During the differentiation process, morphology was routinely evaluated through phase-contrast microscopy (EVOS™ XL Core System, Invitrogen™ 15339661): following their differentiation, cells become progressively more branched and elongated (Figure 10).

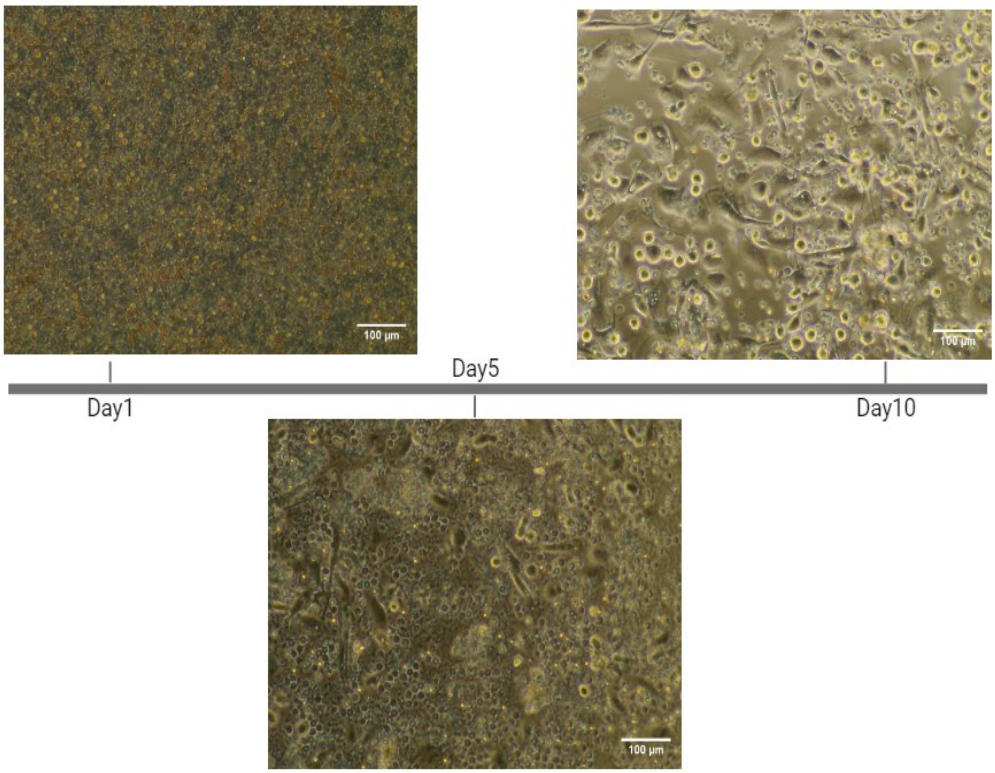

***Figure 10**: Progressive morphological change of cells during differentiation. Phase-contrast microscopy, 20X magnification; scale bar x = 100µm. Created in BioRender.com*

Generally, the differentiation process was completed after 10-14 days; however, some variability was observed between different donors and experiments.

3.2.2 Cellular treatments and medium analysis

Before treatment, the medium was replaced with a stimulation medium, consisting in base RPMI medium supplemented with 1%FBS (see 4.2.1).
For NLRP3 activation, differentiated MDMis were treated with 10ng/ml LPS (Sigma™, 0111:B4) for 3.5h. During the last 30 minutes, 2'(3')-O-(4-benzoylbenzoyl)adenosine-5'-triphosphate (BzATP, Sigma™, B6396) was added to the medium: BzATP is a potent agonist of purinergic P2X7 receptors, which mediates K+ ion efflux and NLRP3 inflammasome assembly. Different dilutions of BzATP were tested in order to obtain a detectable NLRP3 activation and avoid cell death (see 4.2.1).

After stimulation, cell medium was collected and stored at -20ºC for enzyme-linked immonosorbent assay (ELISA).
The medium was specifically analysed for the presence of pro-inflammatory cytokines, using the commercial kits DuoSet Ancillary Reagent Kit (R&D Systems™, DY008), Human IL-1β/IL-1F2 DuoSet (R&D Systems™, DY201-05) and Human TNF-α DuoSet (R&D Systems, DY210-05).

3.2.3 Immunostaining and image analysis

For Immunocytochemistry experiments, after LPS and BzATP stimulation, cells were washed once with PBS. 4% paraformaldehyde (PFA) fixation was performed for 14 minutes at RT and cells were washed three times in PBS.
Cells were incubated for 1h at RT in blocking solution, made up of PBS-Triton 0.3% (Sigma™, T8787) enriched with 0.3M Glycine (Sigma™, G8898) and 5% BSA (Sigma™, A3294).
Then, blocking solution was removed and cells were incubated O/N at 4ºC with primary antibodies, diluted in incubating solution, consisting in PBS-Tween 0.05% (Sigma™, P7949) enriched with 5% BSA. The following antibodies were used: anti-ASC (AdipoGen™, AG-25B-0006-C100) diluted 1:300; anti-IBA1 (Synaptic Systems™, 234009) diluted 1:5000.
The next day, the wells were washed three times with PBS-Tween 0.05% followed by incubation with appropriate fluorophore-conjugated secondary antibodies (anti-chicken Alexa Fluor™ 488, ab150169; anti-rabbit Alexa Fluor™ 555, A32794). Secondary antibodies were diluted 1:1000 in incubating solution. Following incubation (50 minutes, RT, in dark chamber), cells were rinsed three times in PBS-Tween 0.05%. A solution containing DAPI (Abcam™, ab228549) diluted 1:1000 in PBS-Tween 0.05% was then added to the wells to visualize nuclei (10min, RT, in dark chamber). Slides were mounted using Fluoromount-G™ mounting medium (Invitrogen™, 00-4958-02).
The slides were kept O/N at 4ºC to dry.
Image acquisition was performed using an A1R-HD25 Nikon inverted confocal microscope. For each experimental condition, four images were acquired at 40X magnification. Quantification of cells positive for nuclear and cytosolic ASC specks was performed using the ImageJ software cell counter plugin and normalized for the number of nuclei.

3.3 Statistical analysis

GraphPad Prism 10.0.2 software was utilized for conducting statistical analyses. All numerical data are presented as mean ± SEM (standard error of the mean).
The selection of the appropriate statistical test was determined after assessing the normality of the data using the Shapiro-Wilk test. Once a Gaussian distribution was confirmed, a three-way analysis of variance (ANOVA) was employed in immunocytochemistry experiments in mouse model to compare the effects of genotype, brain region, and treatment, as well as their interaction.
For immunocytochemistry experiments and ELISA assays conducted in human model, a two-way ANOVA was employed to compare the effects of genotype and treatment, as well as their interaction.
Post-hoc comparisons were conducted using Šídák's multiple comparisons test.
The following p-values intervals were considered for statistical significance:
0.0332 (*), 0.0021 (**), 0.0002 (***), < 0.0001 (****).

4. Results

4.1 ASC protein specks are more abundant and show a distinct subcellular localization in mouse primary microglia with the G2019S mutation compared to wt microglia

In order to further investigate the dysregulation of the NLRP3 inflammasome activation observed in *LRRK2*-G2019S mouse microglia, an immunocytochemistry experiment was conducted to visualize ASC, the adaptor protein required for NLRP3 inflammasome assembly.

It has been shown that, in resting condition, ASC exhibits a widespread signal localized both in the cytoplasm and the nucleus. However, between the two cellular compartments, ASC levels seem to be more pronounced in the nucleus, which has been suggested to prevent interaction with cytosolic NLRP3 [Bryan et al., 2009].
Under activated conditions, the protein is redistributed in the cell and exported to the cytosol [Bryan et al., 2009].

The objective of this study was to investigate whether primary microglia isolated from the cortical and striatal regions of mice carrying the *LRRK2*-G2019S mutation exhibited increased ASC oligomerization under resting conditions with respect to wt microglia, possibly indicating basal inflammasome activation.

Primary microglia from the two brain regions and genotypes were therefore divided into two groups: a positive control group (LPS + Nigericin, see 3.1.1) and a vehicle-treated group.
Subsequently, image analysis was conducted to separately count cells positive for nuclear and perinuclear/cytosolic ASC specks (representative images in Figure 11). The counts were then normalized to the number of DAPI-positive (DAPI+) nuclei.

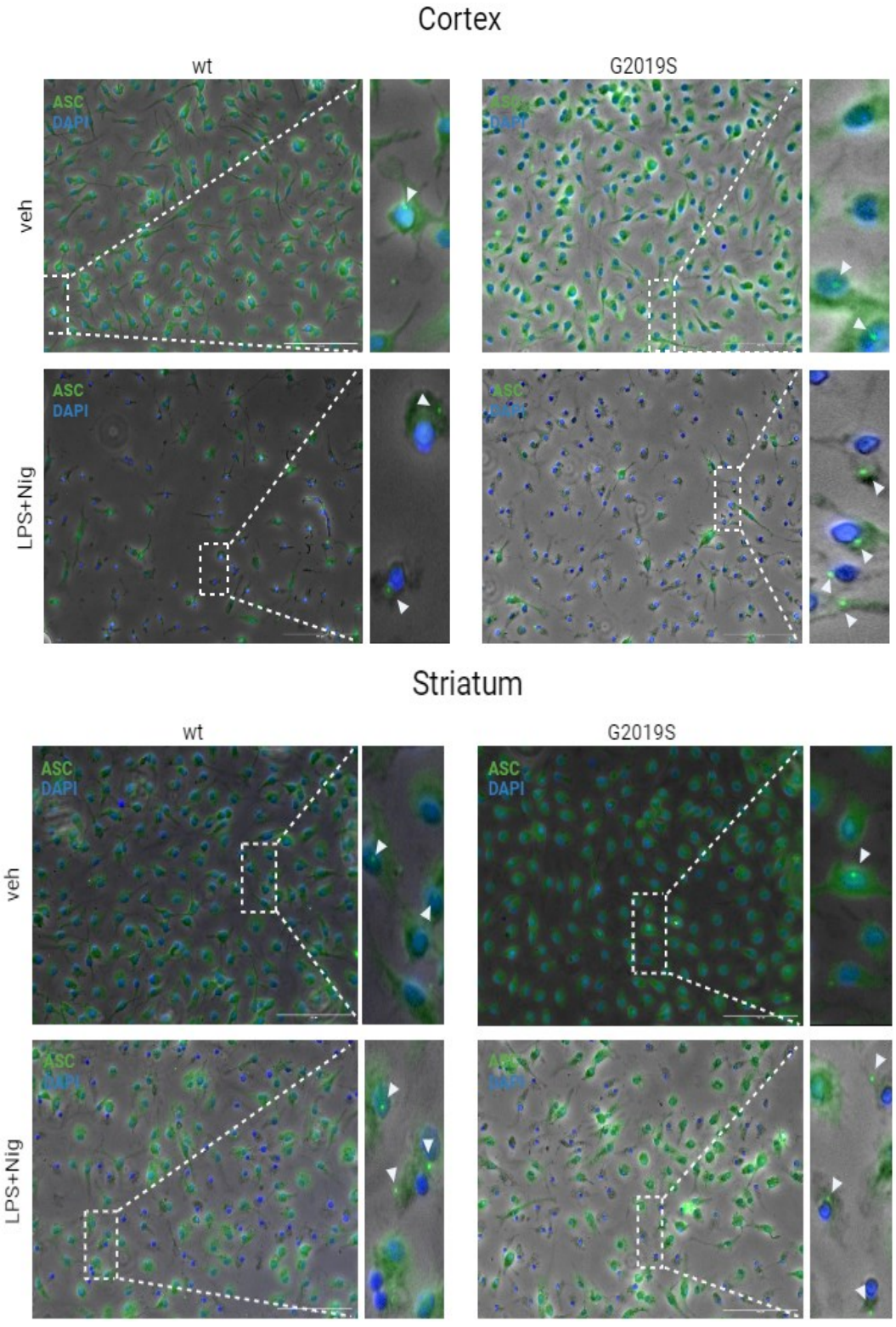

***Figure 11**: wt and Lrrk2-G2019S primary microglia, from cortex or striatum, were treated with DMSO + EtOH (vehicle) or LPS + nigericin and stained with the anti-ASC antibody (green). Cell contour was visualized with bright-field illumination.*

As expected, ASC specks formation was negligible in vehicle-treated wt microglia, whereas exposure to NLRP3 activating agents resulted in increased number of ASC specks, which predominantly localized in the cytosol, independently from genotype and brain region (Figure 12, B).
Interestingly, ASC oligomerization was detected in G2019S microglia even in resting conditions, with a typical localization within the cell nucleus (Figure 12, A).

More in detail, a genotype-dependent upward trend in cells positive to nuclear ASC specks was observed in vehicle-treated cortical microglia, although the wt vs. G2019S comparison did not result in statistical significance ($p = 0.2579$).
Surprisingly, in the striatum both wt and *LRRK2*-G2019S microglia exhibited nuclear ASC oligomerization. Consequently, the genotype effect was less evident for striatal microglia.

In cortical microglia, the response to LPS+Nigericin treatment was more prominent in mutated microglia than in wt microglia ($p < 0.0001$). However, this effect was not found in microglia from the striatum.

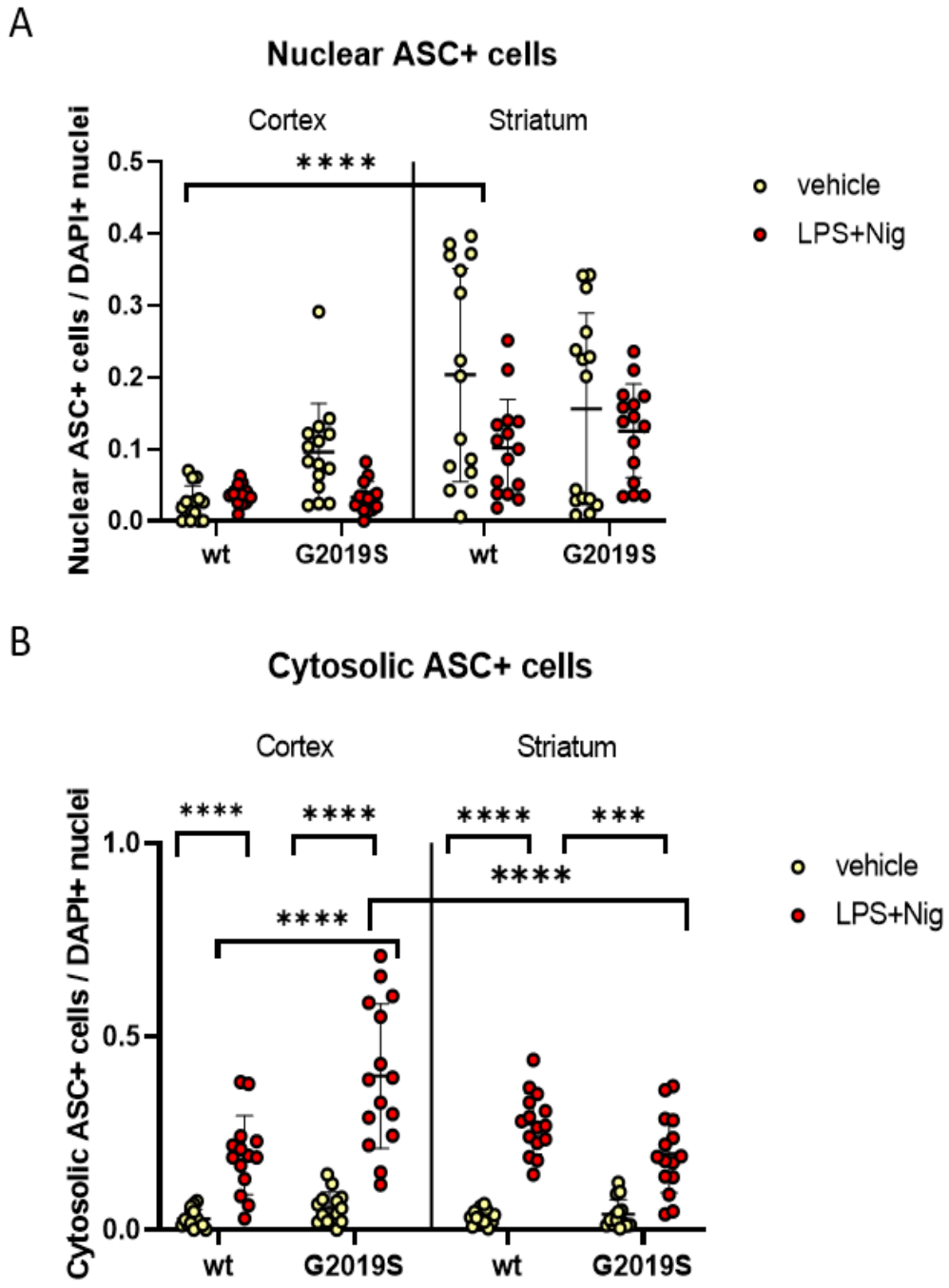

***Figure 12**: Quantification of ASC+ cells in cortical and striatal wt and Lrrk2-G2019S knock-in microglia and corresponding statistical analysis.*

Number of cells with nuclear (A) or cytosolic (B) ASC specks, normalized to total number of DAPI+ nuclei.

Each point in the graph represents the quantification performed on an individual field, acquired from three biological replicates in three independent experiments.

4.2 Validation of a protocol for the efficient activation of the NLRP3 inflammasome in hMDMis

Based on the reported preliminary observations in mouse, the next objective was to confirm the relevance of such findings in a human microglial cell model (see 1.1.4).
PBMCs were isolated, from fresh blood from control individuals through density gradient centrifugation, frozen, thawed and counted, as described above (see 3.2.1). Test experiments were then performed to establish the optimal cell seeding density for differentiation. Optimizations were also performed to establish treatment duration and LPS/BzATP concentrations for the efficient activation of the NLRP3 inflammasome pathway in hMDMis.
Furthermore, the effect on cellular response of FBS supplementation or starvation concomitant to the treatment was tested.

4.2.1 BzATP treatment and effects of starvation on cellular response

Recent work conducted in the lab underlined the need to improve a previously established protocol for hMDMis differentiation.
According to it, in past experiments conducted by the team, PBMCs were seeded at a density of $2*10^6/cm^2$. However, such a high density led to non-optimal differentiation and significant cell loss (about cell seeding density, see 4.2.2). An uncomplete differentiation was evidenced by the lack of the morphological changes indicative of the emergence of the expected microglia-like phenotype, including cellular branching.
Therefore, a preliminary experiment was set in order to test a new seeding density, corresponding to $4.2*10^5/cm^2$.

Following application of the differentiation protocol, hMDMis were treated with 10ng/ml LPS for 3 hours in RPMI medium-1% P/S-1% FBS; subsequently, BzATP was added to the stimulation medium at a dilution of 500µM, for 24 hours.

After 3h of LPS exposure, the cells exhibited the expected morphology, based on the large body of existing literature on microglia [Lambert et al., 2008]. Specifically, while untreated hMDMis initially displayed a bipolar or multipolar appearance, with long and subtle processes, LPS-treated cells exhibited larger and flattened soma, with numerous shorter processes (Figure 13).

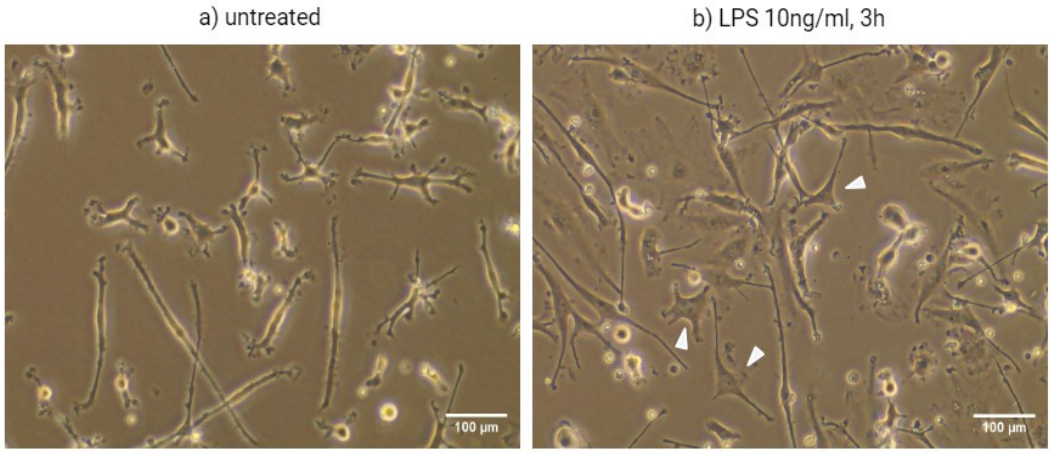

***Figure 13**: Representative micrographs illustrating the morphology of the cells before (a) and after treatment with LPS (b). Phase-contrast microscopy, 20X magnification; scale bar x = 100µm.*

The subsequent treatment with BzATP, on the other hand, killed most of the cells: at this stage, the cells showed the amoeboid morphology typical of activated microglia and detached from the support (Figure 14).

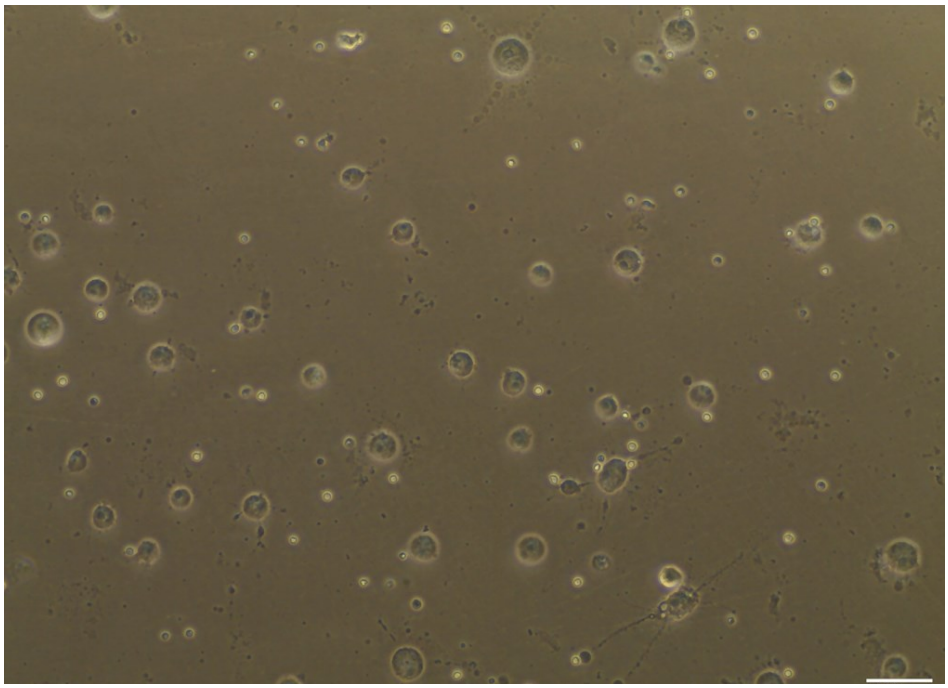

***Figure 14**: Representative illustration of the morphology of the cells after exposure to BzATP (500µM) for 24 hours. Phase-contrast microscopy, 20X magnification; scale bar x = 100µm.*

Under such conditions, PFA fixation and immunostaining were not possible.

This hyper-sensitivity of the cells to the chosen paradigm of NLRP3 inflammasome activation may be linked to the strong decrease operated in cell density compared to the previous protocol. Therefore, it was necessary at this point to determine new parameters for cell stimulation.

Moreover, the presence of 1% FBS in the stimulation medium could be another factor contributing to the observed exacerbated cellular response.
FBS contains a large amount of nutrients necessary for cell growth and activity. On the other hand, cell starvation (consisting in keeping cells in FBS-free medium) is generally used to synchronize cell cycles and remove basal response of cells, when the reaction to a specific treatment is assessed [Sargeant & Fourrier, 2022]. Furthermore, microglial cells in the brain are usually separated from blood serum by the blood-brain barrier. Thus, stimulating hMDMis in medium enriched with FBS does not resemble physiological conditions [Sargeant & Fourrier, 2022].
Therefore, the next experiments were conducted to establish optimal the BzATP concentration and duration of treatment at the new given seeding density of $4.2*10^5/cm^2$. In parallel, the effects of starvation on the cellular response to treatment were also evaluated.

PBMCs from two different healthy donors were used. The differentiation process was induced as described above. At day10, hMDMis from each donor were divided into two groups: the first one treated in FBS-free Base RPMI Medium; the second treated in Base RPMI Medium enriched with 1%FBS. In both cases, the growth medium was removed right before the stimulation and replaced with 500µl of stimulation medium.
Within each group, three different treatments were tested:

- Vehicle-treatment. Cells were kept in the stimulation medium;
- 10ng/ml LPS for 3.5h + BzATP 100µM during the last 30 min;
- 10ng/ml LPS for 3.5h + BzATP 300µM during the last 30 min.

Exposure to BzATP for a duration of 30min was decided based on the previous literature describing stimulation of human microglia [Janks et al., 2018; Rampe et al., 2004]. The indicated papers suggest for example to use a BzATP concentration of 300µM following LPS priming of the cells to activate the NLRP3 inflammasome pathway. Additionally, Francistiová et al. (2022) pointed out that a 24h exposure of human iPSC-derived microglia-like cells to 300µM or 500µM BzATP induces high mortality. Therefore, based on the strong cellular response previously observed, a treatment with BzATP at 100µM was included for testing.

Some differences between groups (-FBS and +FBS) and treatments (BzATP 100µM and BzATP 300µM) were already detectable based on morphological features of the cells (Figure 15).
Exposure to 100µM BzATP produced signs of activation, illustrated by the amoeboid appearance of the cells, whether with or without FBS in the stimulation medium; however, a lower relative number of amoeboid cells was present in conditions without FBS, in which most of the cells conserved the branched morphology characteristic of resting microglia.
Increasing the BzATP concentration to 300µM led to major morphological changes in both groups, suggesting a dose-dependent reaction of cells to BzATP.

However, while in conditions with FBS almost all the cells exhibited an amoeboid morphology, in the group stimulated in FBS-free medium a ramified morphology was still widespread.
Some cells detached during treatment (activated microglia and dead cells both become more prone to detachment), especially in the +FBS condition, but without having a significant impact on the overall cellular density.

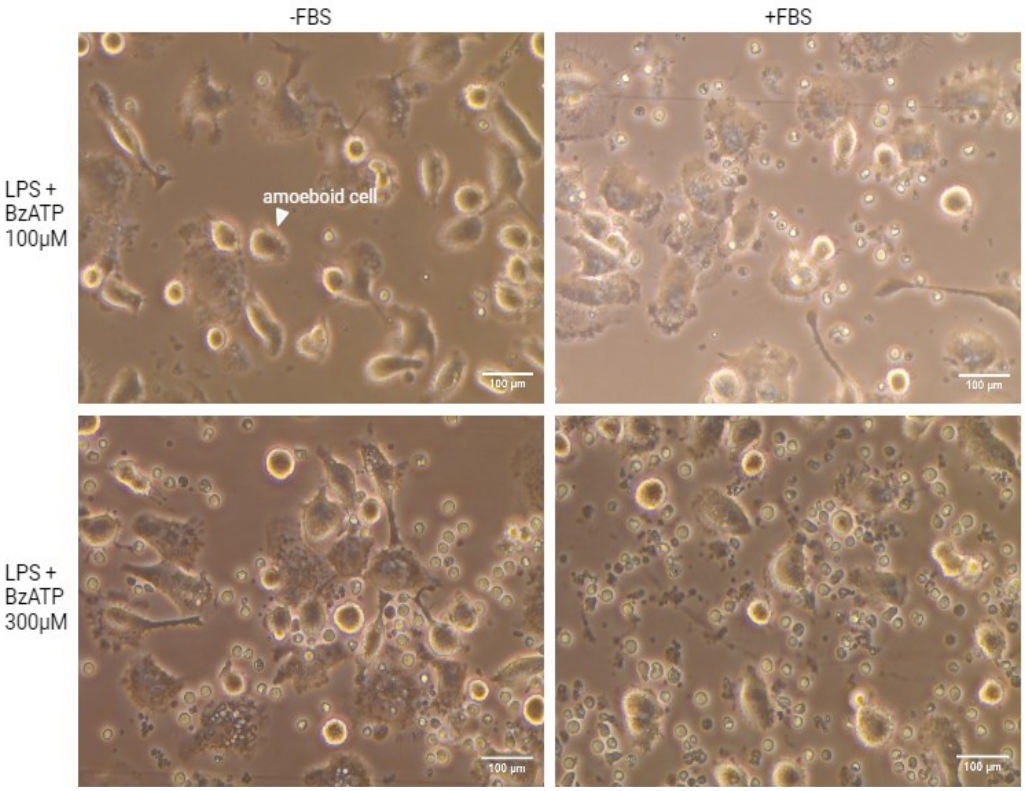

***Figure 15**: Morphological comparison between the two groups (-FBS and +FBS) and treatments (BzATP 100µM and BzATP 300µM).*

Cells were subsequently fixed with PFA and immunostained for ASC and IBA-1; the percentage of cells positive for cytosolic ASC specks was quantified as described above (see 4.1), to evaluate NLRP3 inflammasome activation.
In parallel, an ELISA assay was performed on the collected stimulation medium in order to measure IL1β and TNFα release in vehicle vs. treated conditions.

Examples of microscopy acquisitions illustrating the morphological and immunocytochemical appearance of the cells, and used for the quantitative analysis, are provided in Figure 16.

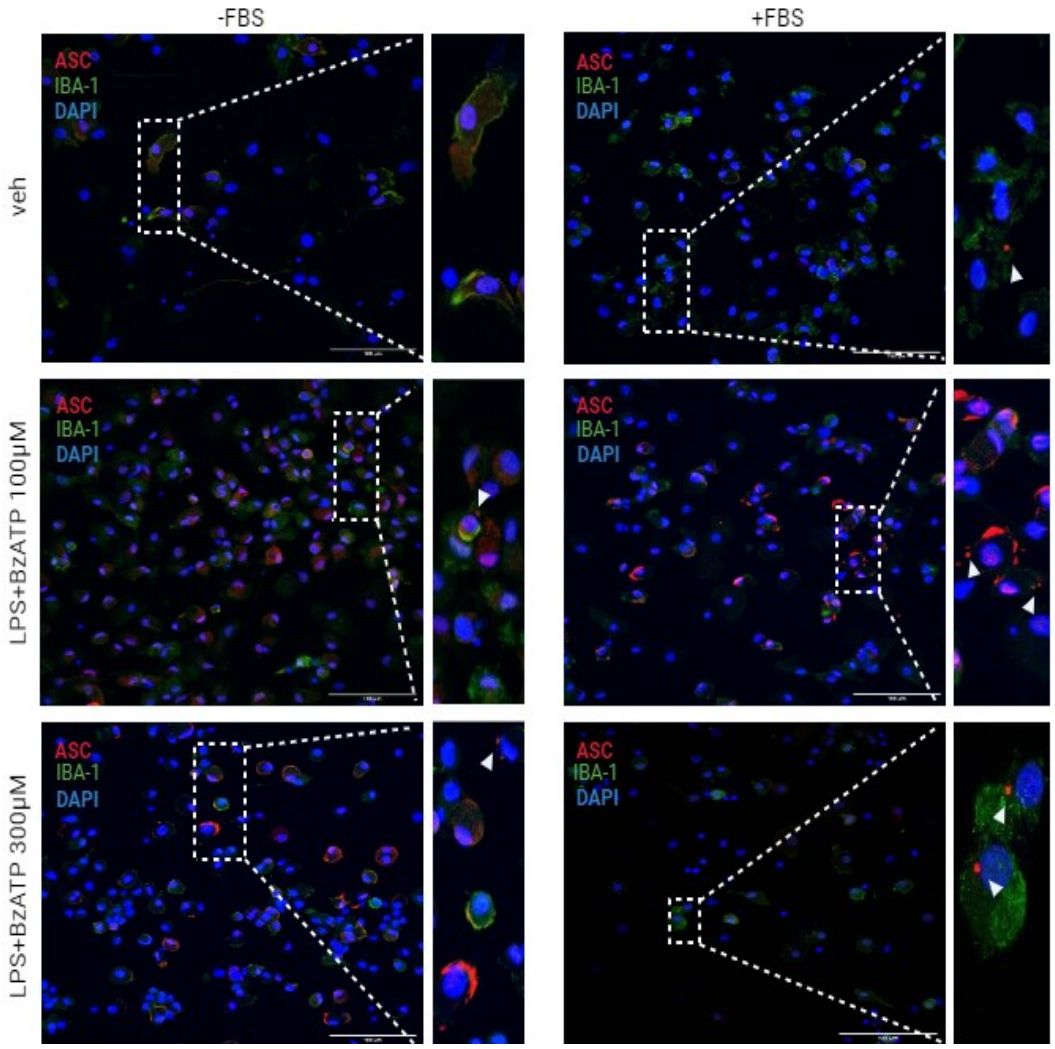

***Figure 16**: Representative images illustrating ASC (red) and IBA1 (green) immunostaining. Scale bar x = 100µm.*

The immunocytochemistry experiment confirmed that both treatments used for NLRP3 inflammasome pathway activation produced an increase in the percentage of cells presenting cytosolic ASC specks, compared to the control condition (Figure 17). However, a significant increase was only detected in the +FBS group ($p < 0.0001$), while only the treatment with BzATP at the concentration of 300µM led to a weakly significant effect in the –FBS group ($p = 0.04$). A trend towards a dose-dependent effect, albeit not statistically significant, was also observed.
Moreover, when comparing the effect of the same treatment between groups, the proportion of cells with cytosolic ASC specks was higher for the stimulation in presence of FBS. Such an effect was only significant for the BzATP concentration of 300µM ($p = 0.0014$).

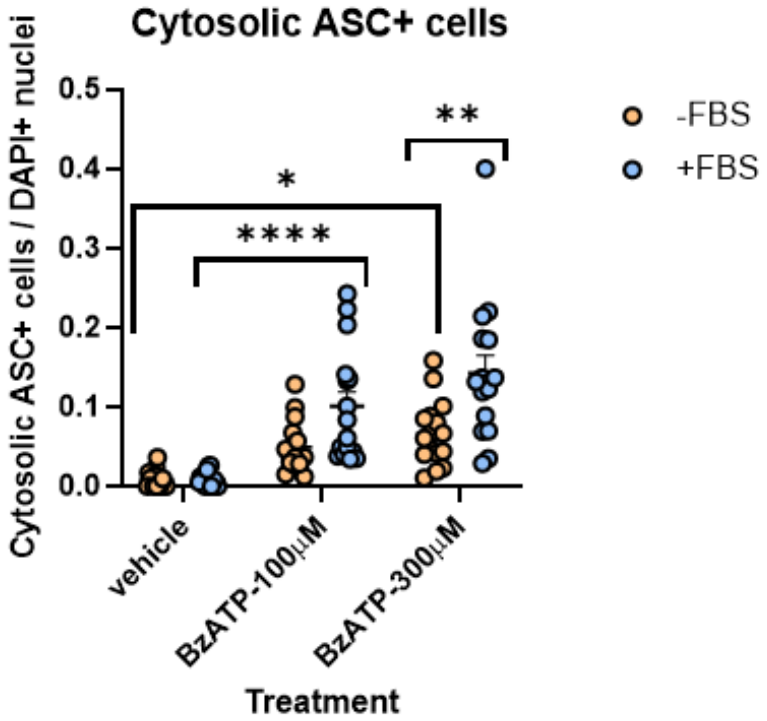

***Figure 17**: Quantification of the proportion of cells positive for cytosolic ASC specks and corresponding statistical analysis. Each point in the graph represents results from an individual field, acquired from two biological replicates in two independent experiments.*

The detection of cytokines release turned out to be problematic for both IL1β and TNFα (Figure 18), likely due to the low cell density at seeding (and the associated poor concentration of the cytokines in the medium). Particularly for IL1β, most of the measurements provided null values, regardless of the treatment parameters, with sporadic outliers detected especially in the +FBS group (Figure 18, A). Some TNFα release was consistently measured in the +FBS group, although with high variability in terms of concentrations (Figure 18, B).

Together, these results confirm the decrease in cellular response already anticipated by cytosolic ASC speck frequency in absence of FBS.

Contrary to what suggested by the morphological analysis of the cells and the immunocytochemistry experiment, there was no indication of dose-dependent effects.

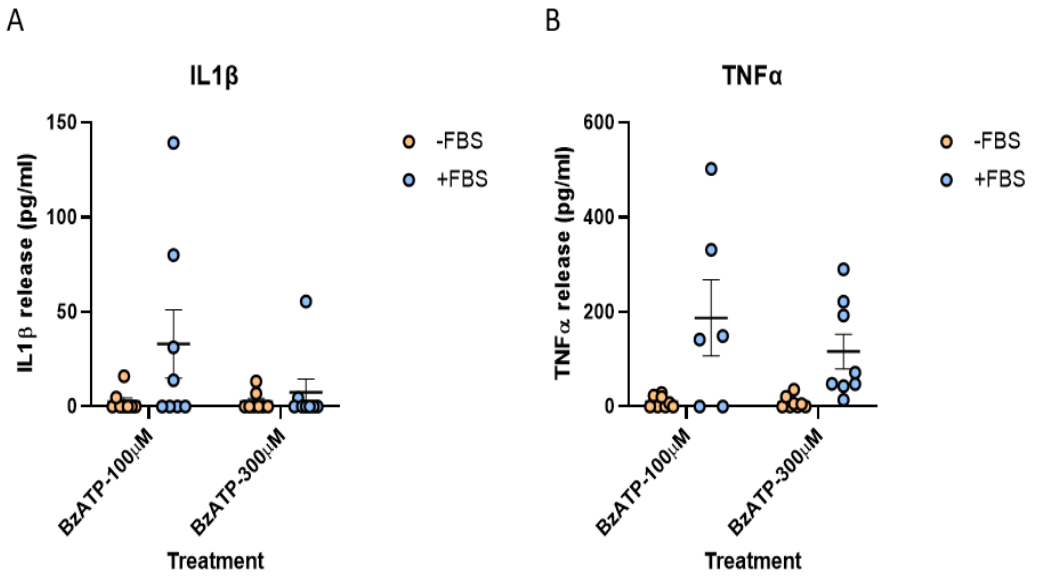

***Figure 18**: IL1β (A) and TNFα (B) release following NLRP3 inflammasome pathway activation. Each point in the graph represents the measurement taken from an independent replicate, obtained from two biological replicates in two independent experiments. Results for vehicle-treated cells were not plotted on the graph in order to facilitate its readability, as they were always equal to 0.*

Overall, these results indicate that adding 1% FBS to the stimulation medium was necessary to obtain a consistently detectable cellular response to the chosen activation paradigms.

Regarding the BzATP stimulation paradigm, using a 300µM concentration for a duration of 30min appeared to be the optimal solution. Indeed, even though a 100µM concentration produced signs of NLRP3 inflammasome activation, the cells reacted in a dose-dependent manner, suggesting that increasing the BzATP concentration would allow to obtain more easily readable results in subsequent experiments.

In order to obtain a double read-out for NLRP3 inflammasome activation, optimizing the conditions for the coherent detection of cytokine release following activation appeared however essential at this stage.

Another experiment was therefore performed, to further adjust the cell seeding density and assay conditions for the detection of cytokines.

4.2.2 Determining the optimal cell seeding density for cytokine detection

Establishing the optimal seeding density of PBMCs is fundamental to maintain the cells in a healthy state, allow them to effectively adhere to the support and induce an effective and uniform differentiation process.

In order to establish the ideal cell seeding density, the previously validated protocol for NLRP3 inflammasome activation (see 4.2.1) was applied in two independent experiments, including a vehicle-treated group (cells kept in the stimulation medium) for each tested density. Cells from two different healthy donors were used. Three different cell seeding density were tested:

- $4.2*10^5$cells/cm^2, corresponding to the previously used density;
- $8.4*10^5$cells/cm^2;
- $1.68*10^6$cells/cm^2. Such a density, which is near to the one used in the initial protocol, was included to confirm the need for adjusting this parameter.

The differentiation process progressed more slowly for the highest density and at day10 the relative number of microglia-like cells was lower compared to the other densities (Figure 19). An optimal differentiation was observed for the density of $8.4*10^5$cells/cm^2.

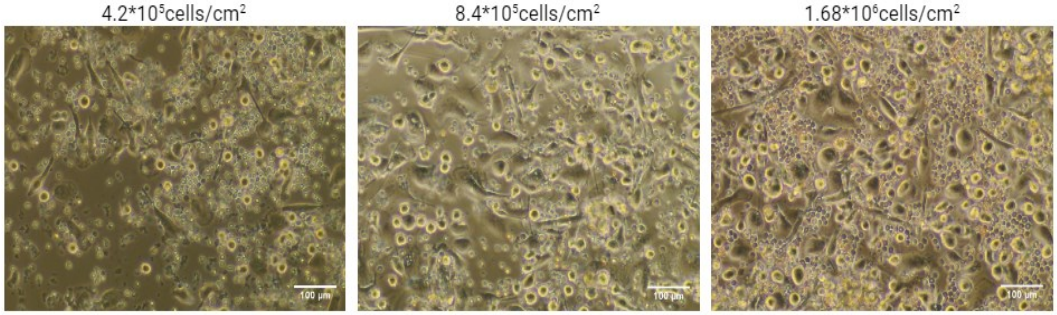

***Figure 19**: Morphological comparison of the hMDMis obtained after seeding PBMCs at three different densities. Pictures were acquired at day10. Phase-contrast microscopy, 20X magnification; scale bar x = 100µm.*

Figure 20 summarizes the results obtained from the immunocytochemistry and ELISA assays performed on the cells following activation.

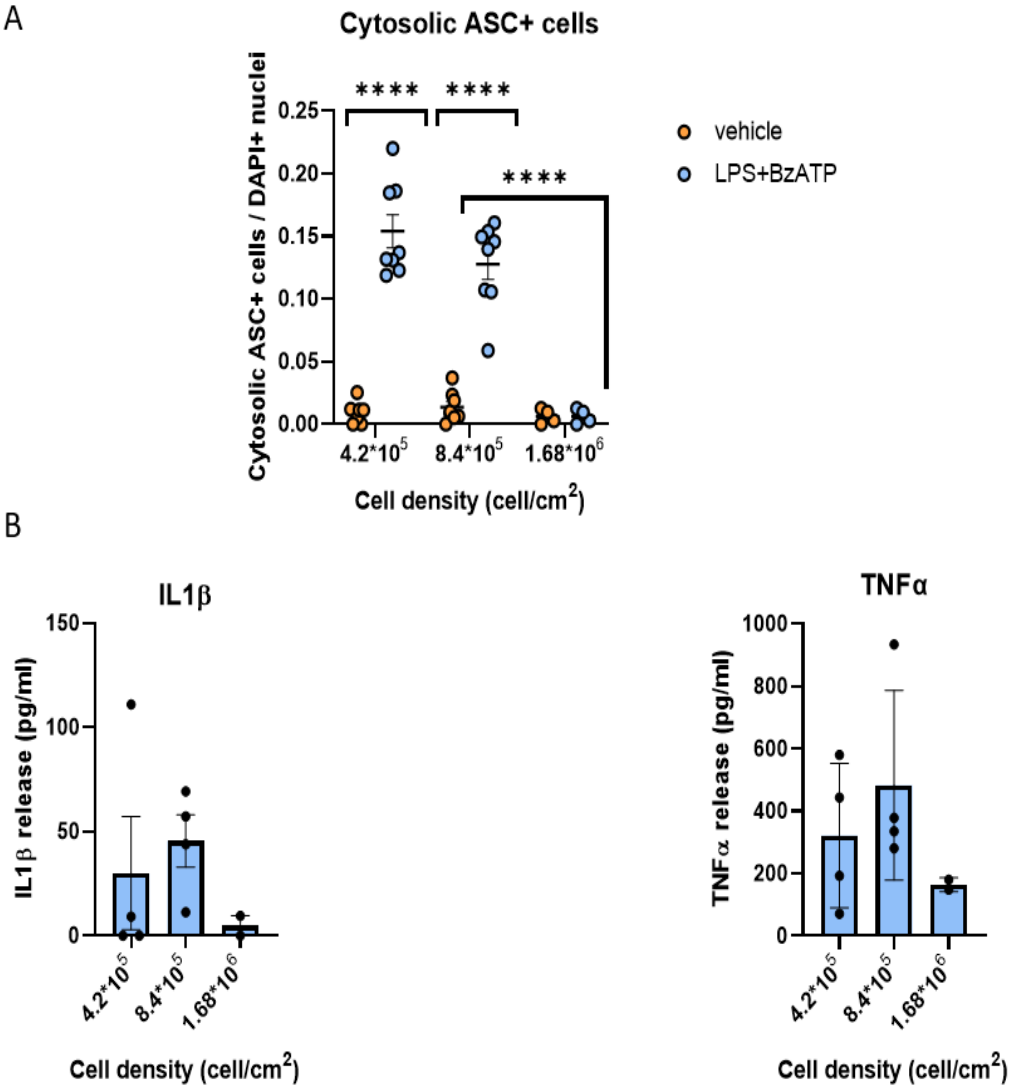

***Figure 20**: Quantification of the proportion of cells presenting cytosolic ASC specks and assay for cytokines release, and corresponding statistical analyses. Each point in the graph represents results from A) an individual field or B) an independent replicate, acquired from two biological replicates in two independent experiments. No statistical analysis was possible, due to the low sample size and variability between values.*

The counting of cells positive for cytosolic ASC specks (Figure 20, A) revealed a significant effect of treatment for the $4.2*10^5$cells/cm^2 and $8.4*10^5$cells/cm^2 densities. For the $1.68*10^6$cells/cm^2 density, no substantial sign of NLRP3 activation was observed.

The average proportion of cells with cytosolic ASC specks tended to be higher for the $4.2*10^5$cells/cm^2 density than for the $8.4*10^5$cells/cm^2 density, but this may

depend on the relatively lower number of cells counted per each acquisition, overall reducing counting reliability.

On the other hand, cytokine release was again much more variable for the $4.2*10^5$cells/cm^2 density, with both IL1β and TNFα release lower on average than for the $8.4*10^5$cells/cm^2 density (Figure 20, B).

IL1β release was almost no detectable for the $1.68*10^6$cells/cm^2 density.

Taken together, these results suggest that a density of $8.4*10^5$cells/cm^2 is optimal for the reliable detection of both changes to cytosolic specks formation and release of cytokines in the considered activation paradigm.

4.3 LPS priming of the NLRP3 inflammasome pathway leads to increased ASC oligomerization within the nucleus of hMDMis

Previous results obtained in mouse highlighted that an important proportion of wt striatal microglia, as well as *LRRK2*-G2019S cortical microglia, exhibit nuclear ASC specks under resting conditions. Such a distinct subcellular localization of ASC specks requires further investigation, as it may represent an intermediate step in the activation of the NLRP3 inflammasome pathway.

Three independent experiments were therefore performed to check for potential effects of NLRP3 inflammasome priming on ASC oligomerization.

PBMCs from three different healthy donors were thawed, seeded and differentiated into MDMis according to the established protocol (see 3.2) and chosen parameters (see 4.2).

MDMis from each donor were divided into three different groups, subjected to different treatments:

- vehicle: cells were kept in the stimulation medium;
- LPS (10ng/ml for 3.5 hours), used as a priming stimulus;
- LPS+BzATP (see 4.2.1): this treatment was included as a positive control for activation of the NLRP3 inflammasome pathway.

After treatment, the cells were fixed with PFA and immunostained for ASC and IBA-1.

The widespread signal of ASC increased after treatment with LPS (see Figure 21), especially within the nucleus of the cells, confirming the previously observed upregulation of *ASC* expression following priming of the cells.

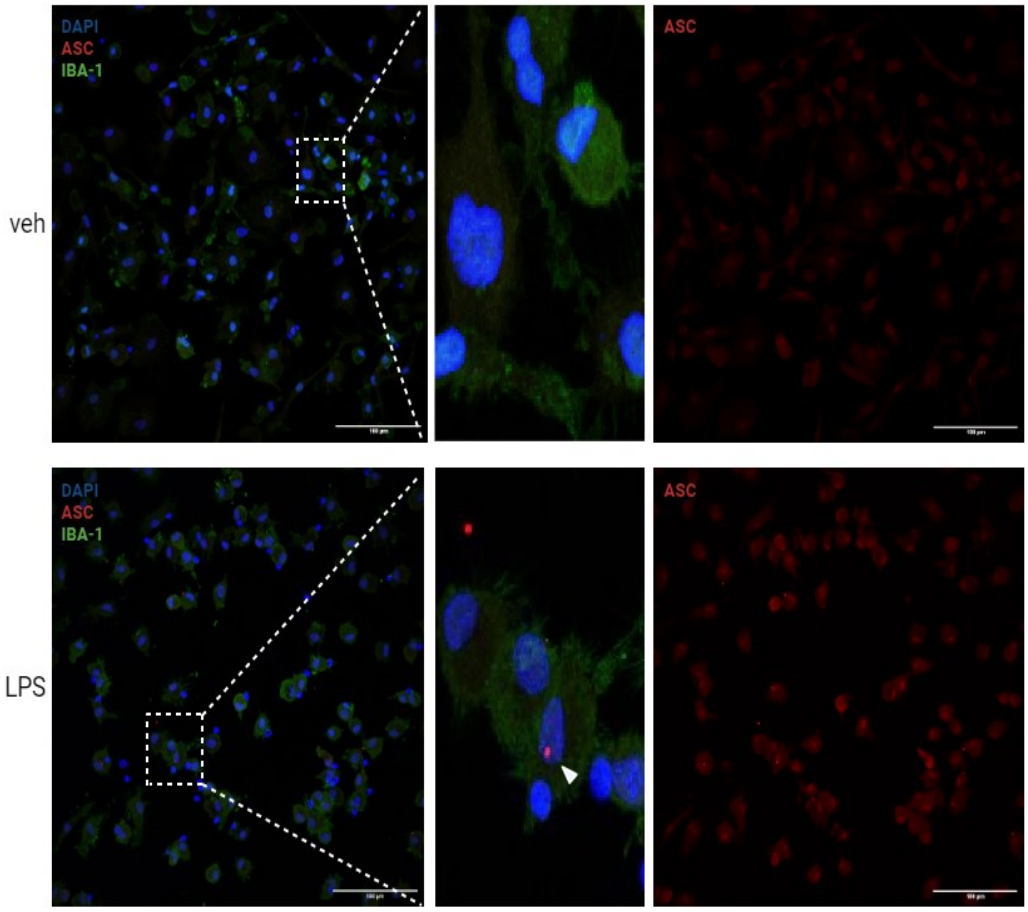

***Figure 21**: Comparison of the immunocytochemical appearance of the cells in the vehicle-treated condition or in the LPS-treated condition. ASC widespread signal showed an increased intensity after treatment with LPS, and ASC specks appeared.*

The quantification of the cells positive for nuclear and cytosolic ASC specks was then conducted as described above (see 3.1.2). Results are summarized in Figure 22.

As expected, the canonical paradigm for the NLRP3 inflammasome pathway activation (LPS+BzATP) produced a significant increase in the proportion of cells exhibiting cytosolic ASC specks ($p < 0.0001$).

Interestingly, after treatment with only LPS, the relative number of cells positive for nuclear ASC specks was significantly higher compared both to vehicle-treated condition ($p < 0.0001$) and to LPS+BzATP-treated condition ($p = 0.0019$).

Within the group of cells treated with LPS, the proportion of cells presenting nuclear ASC specks was higher than the proportion of cells with cytosolic ASC specks ($p = 0.0003$).

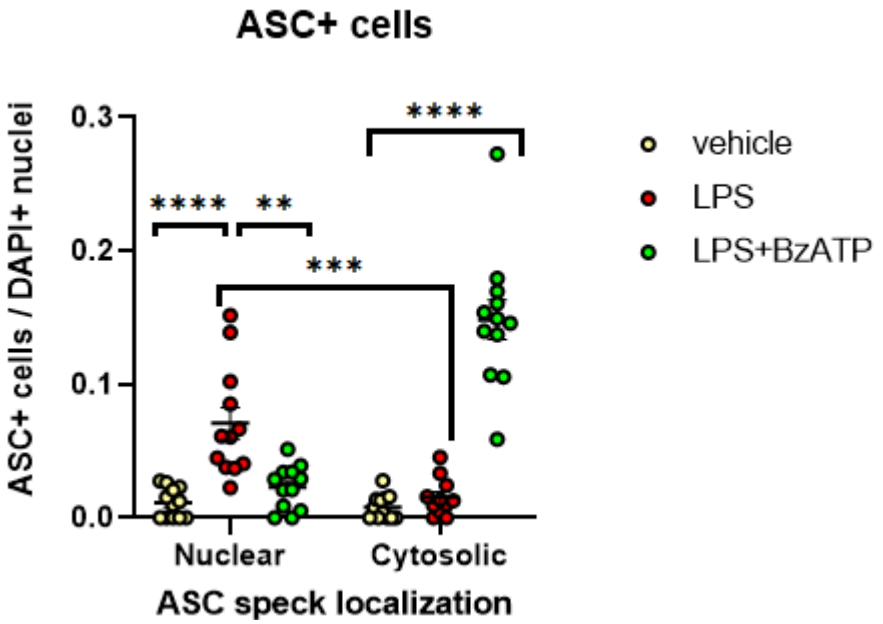

***Figure 22**: Quantification of the proportion of cells presenting nuclear or cytosolic ASC specks, and corresponding statistical analysis. Each point in the graph represents results from an individual field, acquired from three biological replicates in three independent experiments.*

All together, these results indicate that ASC oligomerization occurs within the nucleus after the priming step and before the full activation of the NLRP3 inflammasome in the cytosol. This suggests that the ASC specks formed in the nucleus are possibly transferred to the cytosol in a second step, following the presentation of an activating stimulus.

4.4 ASC specks formation and localization in wt, *LRRK2*-G2019S and *PRKN* mutant hMDMis

As previous experiments highlighted, ASC oligomerization is impaired in cortical *LRRK2*-G2019S mouse primary microglia.

If confirmed in human models, the accumulation of nuclear ASC specks may represent a hallmark of *LRRK2*-PD, indicating an interaction between LRRK2 and the NLRP3 inflammasome pathway. Similar defects in ASC oligomerization could potentially result from mutations in other PD-genes, such as *PRKN*.

A case-control study was conducted to investigate the effect of mutations in *LRRK2* or *PRKN* on ASC speck formation and NLRP3 inflammasome activation, exploiting the hMDMis model. PBMCs from 4 *LRRK2* patients and 2 *PRKN* patients, previously collected and frozen, were thawed; each patient was associated with an age- and sex-matched control (see 3.2.1).

Following application of the differentiation protocol as described above, hMDMis from each subject were divided into three groups and subjected to three treatments: vehicle, LPS and LPS + BzATP (see 4.3).

An exacerbated response to BzATP exposure was observed in mutant hMDMis from both *LRRK2* and *PRKN* patients compared to the respective control cells (despite the high interindividual variability), resulting in significant cell death and detachment.

After fixation with PFA and immunostaining for ASC and IBA-1, the proportion of cells positive for nuclear and cytosolic ASC specks was quantified.

Within the nucleus (results summarized in Figure 23), ASC specks under basal conditions was more abundant in *LRRK2*-G2019S cells compared to wt ($p = 0.0086$. Figure 23, b), while ASC oligomerization in *PRKN*-mutant cells did not change comparatively to controls. The proportion of cells presenting nuclear ASC specks significantly increased after LPS exposure in hMDMis from all the genotypes, but both *LRRK2*- and *PRKN*-mutant cells showed a lower number of ASC specks compared to wt cells. The percentage of cells positive for nuclear ASC specks consistently decreased after BzATP exposure, resulting in statistical significance regardless of the genotype.

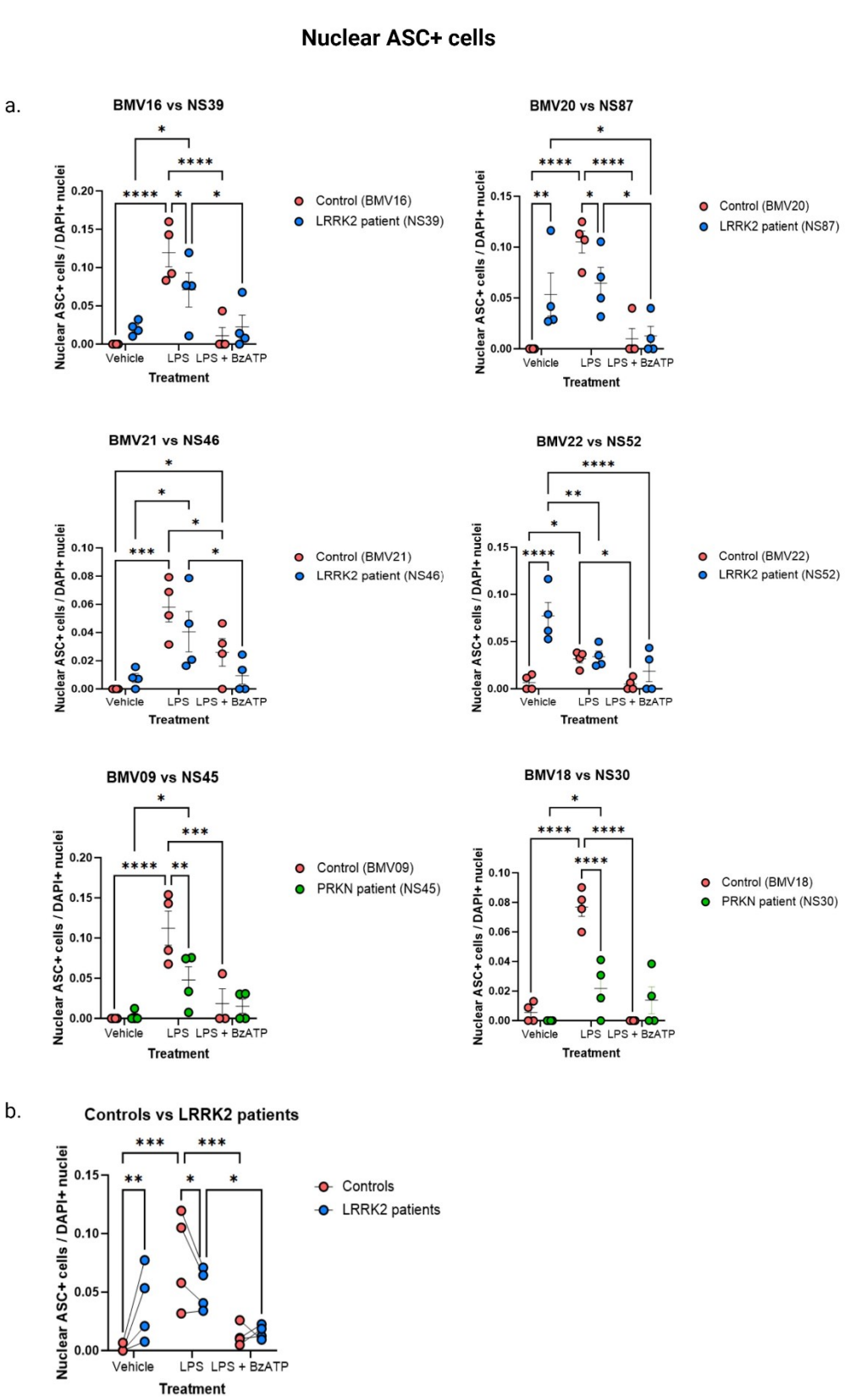

***Figure 23**: Quantification of the proportion of cells presenting nuclear ASC specks, and corresponding statistical analysis. Each point in the graph represents a) results from an individual field, acquired from each individual within a control-patient pair or b) the mean value for each individual, calculated taking into account four fields per individual.*

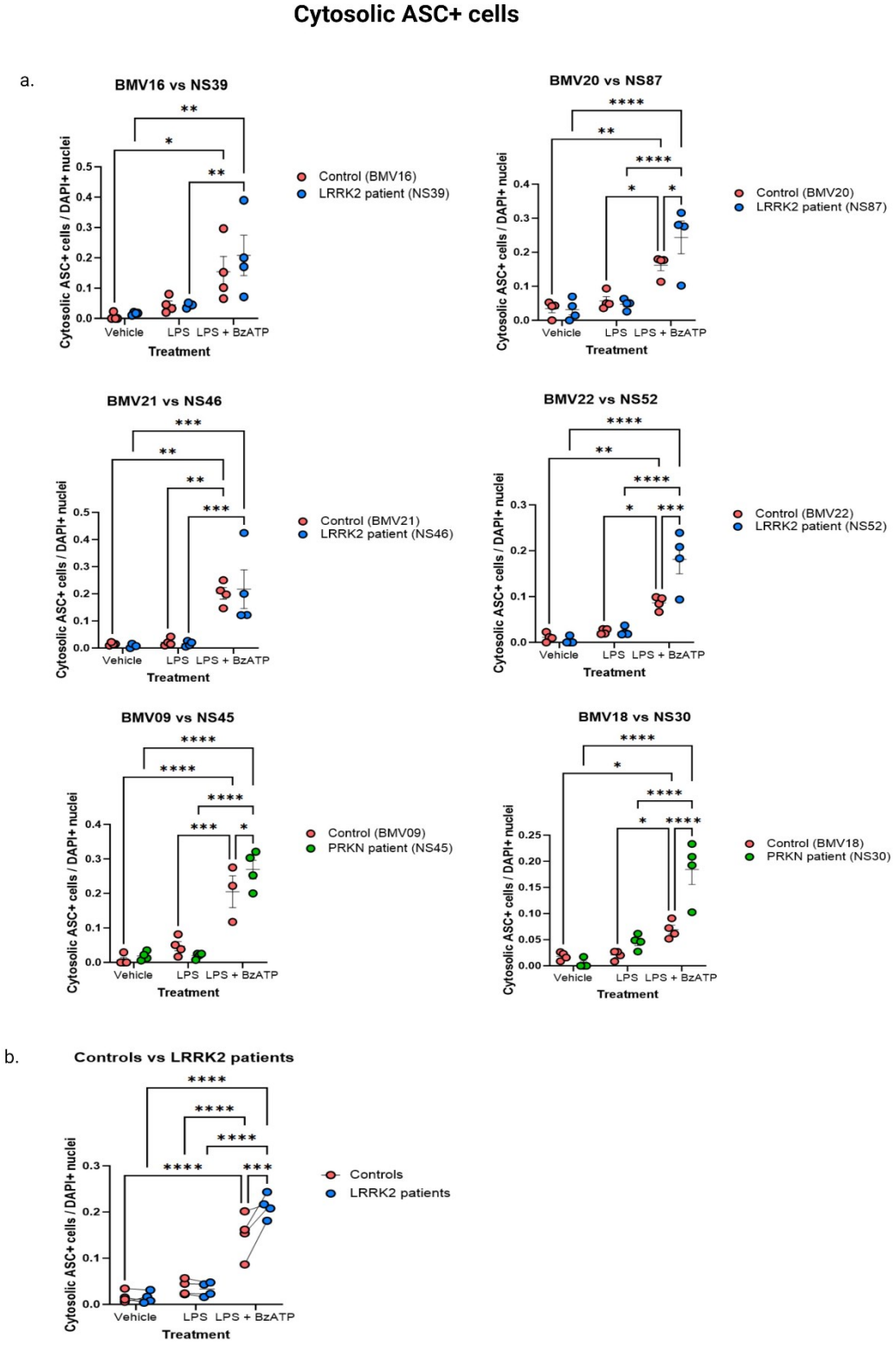

***Figure 24**: Quantification of the proportion of cells presenting cytosolic ASC specks, and corresponding statistical analysis. Each point in the graph represents a) results from an individual field, acquired from each individual within a control-patient pair or b) the mean value for each individual, calculated taking into account four fields per individual.*

On the other hand, LPS + BzATP treatment produced a significant increase in the number of cells presenting cytosolic ASC specks, irrespective of the genotype, while LPS treatment did not result in significant cytosolic ASC oligomerization (Figure 24). Interestingly, a more emphatic response to BzATP was measured in both *LRRK2*- ($p = 0.0002$. Figure 24, b) and *PRKN*-mutant cells compared to wt cells ($p = 0.0438$ and $p < 0.0001$), despite high interindividual variability.

In parallel to immunocytochemistry experiment, the stimulation medium was collected, and an ELISA assay was conducted to quantify the release of IL1β and TNFα. Considering the detachment of the cells observed for hMDMis from PD patients after exposure to LPS + BzATP, a normalization was applied to correct for the number of cells. In particular, four acquisitions were systematically taken from each well under confocal microscopy at 20X magnification, and IBA-1 positive cells were counted. The cytokine concentrations measured for treated conditions were then normalized based on the average cell density counted for the corresponding vehicle condition. The results of this analysis are summarized in Figure 25 and Figure 26.

Mutations in both the PD-linked genes were associated with increased release of IL1β following treatment with LPS + BzATP (Figure 25), indicating overactivation of the NLRP3 inflammasome pathway consistent with the corresponding increase in cytosolic ASC specks.
On the contrary, no significant genotype-dependent effect was detected concerning TNFα release (Figure 26). The difference in released TNFα concentrations, observed in some cases between the LPS and LPS + BzATP conditions and significant for some of the control-*LRRK2* patient pairs (specifically, the BMV16-NS39 and BMV22-NS52 pairs. Figure 26, a), does not result in statistical significance in the global analysis.

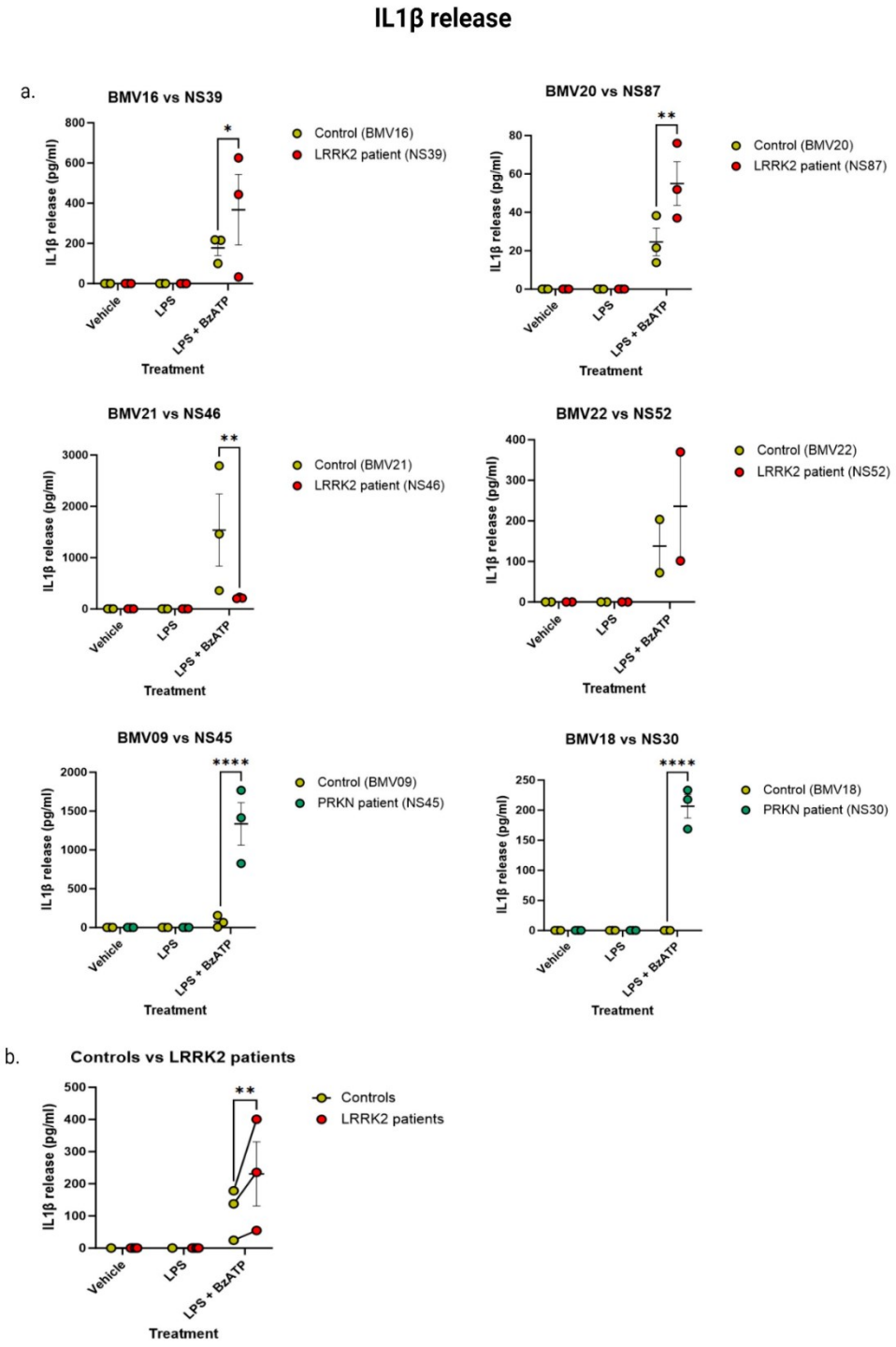

***Figure 25**: Assay for IL1β release, and corresponding statistical analyses. Each point in the graph represents results from a) an independent replicate, acquired from each individual within a control-patient pair or b) the mean value for each individual, calculated based on three independent replicates.*

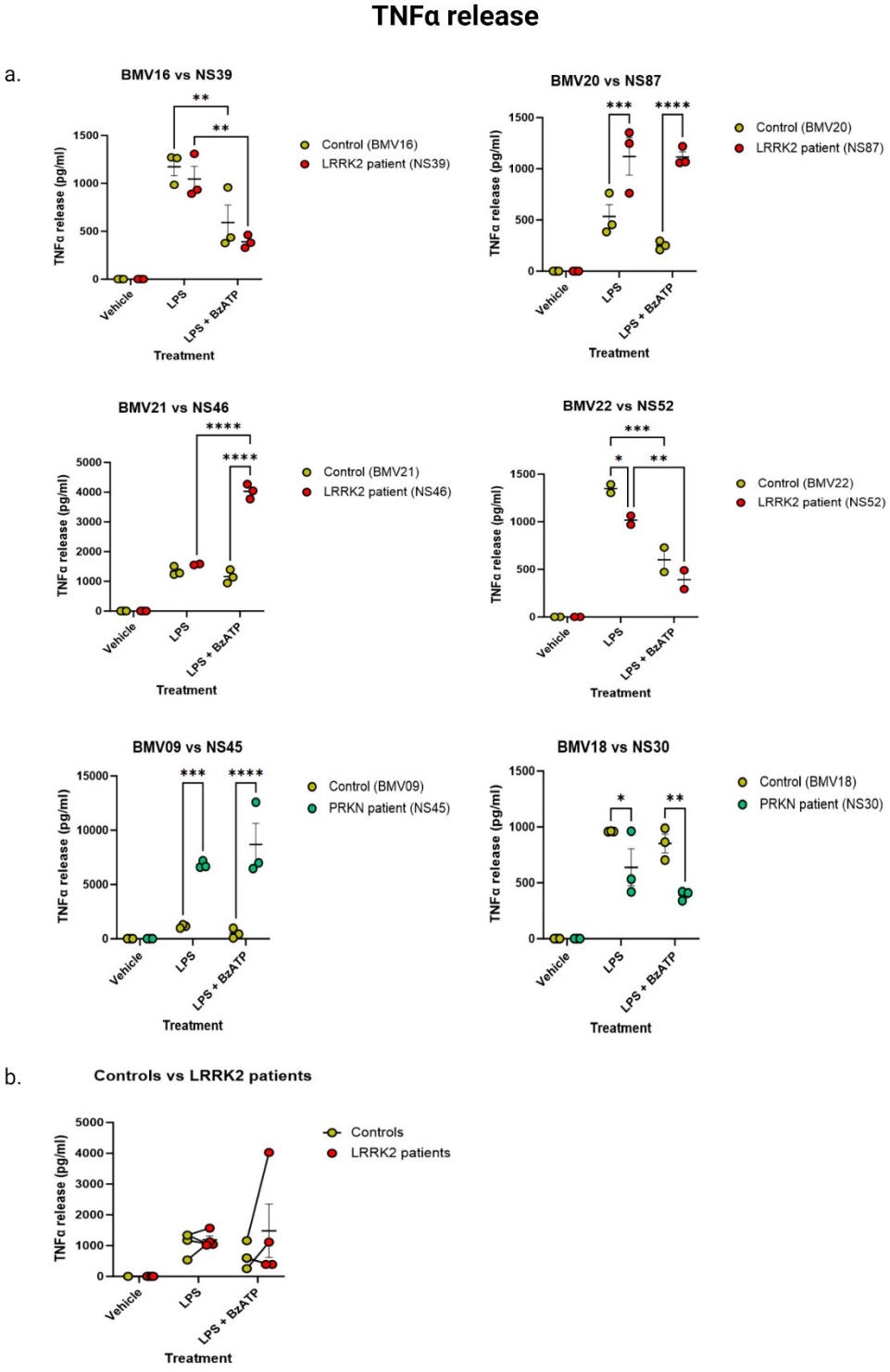

Figure 26*: Assay for TNFα release, and corresponding statistical analyses. Each point in the graph represents results from a) an independent replicate, acquired from each individual within a control-patient pair or b) the mean value for each individual, calculated based on three independent replicates.*

5. Discussion

Microglia, representing the resident immune cells in the CNS and the primary mediators of neuroinflammatory processes, play a pivotal role in the progression of neurodegenerative disorders, such as PD [Kwon & Koh, 2020].
So far, most of the studies investigating the involvement of microglia in the pathophysiology of PD were conducted in mouse. However, some comparative studies highlighted that microglia underwent evolutionary changes across vertebrate phylogeny, resulting in morphological and transcriptomic heterogeneity between species [Giersdottir et al., 2019]. Notably, human microglia display a higher heterogeneity compared to all other mammals in terms of gene expression, and among the genes whose expression is enriched, several have been associated to PD susceptibility [Giersdottir et al., 2019].

On these phylogenetic bases, the present study investigates the reliability of results obtained in animal models for PD research, comparing the same experimental setup in mouse and human models.

The chosen hMDMi model provides the possibility to easily and quickly obtain cells with a microglia-like phenotype, but it is mainly limited by the lack of a standardized protocol for their differentiation. Here, new parameters for an efficient differentiation of human blood-derived monocytes into hMDMis are provided.

The results obtained in this study underline the existence of a link between *LRRK2* and NLRP3 inflammasome pathways, conserved between mouse primary microglia and hMDMis and not reported previously in literature. *LRRK2*-G2019S microglia exhibit more cytosolic ASC specks and release higher amounts of IL1β compared to wt cells upon inflammasome activation.
Notably, microglia carrying the G2019S mutation accumulate ASC specks within the nucleus in absence of inflammatory agents, indicating a pre-active basal state of the NLRP3 inflammasome pathway. Conversely, wt microglia exhibit nuclear ASC oligomerization only following LPS treatment, known to prime the NLRP3 inflammasome pathway in preparation for further activating stimuli, which result in ASC relocation to the cytosol.
It is possible that the priming step can be by-passed, and a single activating stimulus leading to K+ efflux (e.g., nigericin, BzATP or α-synuclein) may be enough to trigger NLRP3 activation in mutant microglia. However, such a possibility, together with the exact ASC oligomerization dynamics, need to be investigated in future experiments.

The presence of significant numbers of nuclear ASC specks was also observed under resting conditions in striatal primary microglia from wt mice. Although the nature of the chosen model did not allow to validate this result in humans, it may be indicative of the regional heterogeneity of microglia. Since the striatum receives nigrostriatal afferences from the SNpc, a dysregulated NLRP3 inflammasome activation in this region could be implicated in the retrograde

axonal degeneration manifesting early in PD.

Previous studies from the team at the Paris Brain Institute [Mouton-Liger et al., 2018] have demonstrated that NLRP3 inflammasome overactivation is involved in *PRKN*-PD too. Such a result was confirmed in the present study, by the observation of higher IL1β release in cells with *PRKN* mutations than in cells from control individuals following activation of the pathway. In addition, second evidence of the hyperresponsiveness of this pathway in microglia from individuals with *PRKN* mutations is provided by the increase in cytosolic ASC specks, reported here for the first time, assuming that formation of such specks is an indicator of NLRP3 inflammasome assembly.
However, the absence of nuclear ASC specks under basal conditions in *PRKN* patients indicates that mutations in *PRKN* and *LRRK2* impact different molecular steps across the process of NLRP3 inflammasome activation.
Further investigations are required to dissect such molecular steps. For instance, the significance of the decreased ASC oligomerization within the nucleus of *LRRK2*- and *PRKN*- mutant microglia following priming with LPS is to be clarified in future research.
A screening study with higher sample size would also be useful to confirm the findings of this study.

Overall, these results support the translational value of studies conducted in mouse regarding the NLRP3 inflammasome pathway in microglia, and propose that overactivation of this pathway is a pathophysiological hallmark of the two most common familial forms of PD.
Targeting ASC oligomerization or redistribution holds promise for the treatment of familial and possibly idiopathic PD.

References

Bloem, B. R., Okun, M. S., & Klein, C. (2021). Parkinson's disease. The Lancet, 397(10284), 2284-2303.

Dorsey, E. R., Sherer, T., & Okun, M. S. (2018). The emerging evidence of the Parkinson pandemic. Journal of Parkinson's Disease, 8(s1), S3-S8.

Fan, J., Chen, S., Zhang, J., & Huang, X. (2021). Alpha-synuclein and cognitive decline in Parkinson disease. Frontiers in Aging Neuroscience, 13, 699701.

Iannotta, L., & Greggio, E. (2021). LRRK2 signaling in neurodegeneration: two decades of progress. Journal of Parkinson's Disease, 11(2), 467-488.

Jewell, C., O'Brien, E., & Hu, M. T. (2022). Inflammasome activation in Parkinson's disease. Journal of Neuroinflammation, 19(1), 19.

Poewe, W., Seppi, K., Tanner, C. M., Halliday, G. M., Brundin, P., Volkmann, J., ... & Lang, A. E. (2017). Parkinson disease. *Nature reviews Disease primers*, *3*(1), 1-21.

Lees, A. J., Hardy, J., & Revesz, T. (2009). Parkinson's disease. The Lancet, 373(9680), 2055-2066.

Bhidayasiri, R., Tarsy, D., & Simon, D. K. (2013). Movement disorder emergencies. Springer Science & Business Media.

Parkinson, J. (2002). An essay on the shaking palsy. Journal of Neuropsychiatry and Clinical Neurosciences, 14(2), 223-236.

Fearnley, J. M., & Lees, A. J. (2019). Ageing and Parkinson's disease: substantia nigra regional selectivity. Brain, 142(12), 3247-3257.

Ovallath, S., & Deepa, P. (2013). The history of parkinsonism: descriptions in ancient Indian medical literature. *Movement Disorders*, *28*(5), 566-568.

G.Berrios & R.Landau. From Kamnos to Parkinson's Disease: The History of Parkinsonism. (2016) Movement Disorders 2016 (Volume 31, Issue 9)

Ascherio, A., & Schwarzschild, M. A. (2016). The epidemiology of Parkinson's disease: risk factors and prevention. *The Lancet Neurology*, *15*(12), 1257-1272.

Checkoway, H., Powers, K., & Smith-Weller, T. (1999). Epidemiologic approaches to the study of Parkinson's disease etiology. Epidemiologic reviews, 21(2), 181-196.

D. W. Dickson. Parkinson’s disease and parkinsonism: Neuropathology. Cold Spring Harbor Perspectives in Medicine, 2:a009258–a009258, 8 2012.

Corti, O., Lesage, S., & Brice, A. (2011). What genetics tells us about the causes and mechanisms of Parkinson's disease. *Physiological reviews*.

Emin, D., Zhang, Y. P., Lobanova, E., Miller, A., Li, X., Xia, Z., ... & Klenerman, D. (2022). Small soluble α-synuclein aggregates are the toxic species in Parkinson’s disease. *Nature communications*, *13*(1), 5512.

Goedert, M. (2001). Alpha-synuclein and neurodegenerative diseases. *Nature reviews neuroscience*, *2*(7), 492-501.

Jenner, P. (2003). Oxidative stress in Parkinson's disease. *Annals of Neurology: Official Journal of the American Neurological Association and the Child Neurology Society*, *53*(S3), S26-S38.

Schapira, A. H. V., Cooper, J. M., Dexter, D., Clark, J. B., Jenner, P., & Marsden, C. D. (1990). Mitochondrial complex I deficiency in Parkinson's disease. *Journal of neurochemistry*, *54*(3), 823-827.

McGeer, P. L., Itagaki, S., Boyes, B. E., & McGeer, E. G. (1988). Reactive microglia are positive for HLA-DR in the substantia nigra of Parkinson's and Alzheimer's disease brains. *Neurology*, *38*(8), 1285-1285.

Kettenmann, H., Hanisch, U. K., Noda, M., & Verkhratsky, A. (2011). Physiology of microglia. *Physiological reviews*, *91*(2), 461-553.

Paolicelli, R. C., Sierra, A., Stevens, B., Tremblay, M. E., Aguzzi, A., Ajami, B., ... & Wyss-Coray, T. (2022). Microglia states and nomenclature: A field at its crossroads. *Neuron*, *110*(21), 3458-3483.

Ginhoux, F., Greter, M., Leboeuf, M., Nandi, S., See, P., Gokhan, S., ... & Merad, M. (2010). Fate mapping analysis reveals that adult microglia derive from primitive macrophages. *Science*, *330*(6005), 841-845.

McGeer, P. L., Itagaki, S., Boyes, B. E., & McGeer, E. G. (1988). Reactive microglia are positive for HLA-DR in the substantia nigra of Parkinson's and Alzheimer's disease brains. *Neurology*, *38*(8), 1285-1285.

Aldana, B. I. (2019). Microglia-specific metabolic changes in neurodegeneration. *Journal of molecular biology*, *431*(9), 1830-1842.

Kwon, H. S., & Koh, S. H. (2020). Neuroinflammation in neurodegenerative disorders: The roles of microglia and astrocytes. *Translational neurodegeneration*, *9*, 1-12.

Kelley, N., Jeltema, D., Duan, Y., & He, Y. (2019). The NLRP3 inflammasome: an overview of mechanisms of activation and regulation. *International journal of molecular sciences*, *20*(13), 3328.

Hulse, J., & Bhaskar, K. (2022). Crosstalk between the NLRP3 inflammasome/ASC speck and amyloid protein aggregates drives disease progression in Alzheimer's and Parkinson's disease. *Frontiers in Molecular Neuroscience*, *15*, 15.

Zhong, Z., Umemura, A., Sanchez-Lopez, E., Liang, S., Shalapour, S., Wong, J., ... & Karin, M. (2016). NF-κB restricts inflammasome activation via elimination of damaged mitochondria. *Cell*, *164*(5), 896-910.

Zhou, R., Yazdi, A. S., Menu, P., & Tschopp, J. (2011). A role for mitochondria in NLRP3 inflammasome activation. *Nature*, *469*(7329), 221-225.

Kelley, N., Jeltema, D., Duan, Y., & He, Y. (2019). The NLRP3 inflammasome: an overview of mechanisms of activation and regulation. *International journal of molecular sciences*, *20*(13), 3328.

Jewell, S., Herath, A. M., & Gordon, R. (2022). Inflammasome activation in Parkinson's disease. *Journal of Parkinson's disease*, (Preprint), 1-16.

Guo, H., Callaway, J. B., & Ting, J. P. (2015). Inflammasomes: mechanism of action, role in disease, and therapeutics. *Nature medicine*, *21*(7), 677-687.

Muñoz-Planillo, R., Kuffa, P., Martínez-Colón, G., Smith, B. L., Rajendiran, T. M., & Núñez, G. (2013). K+ efflux is the common trigger of NLRP3 inflammasome activation by bacterial toxins and particulate matter. *Immunity*, *38*(6), 1142-1153.

Grosso, G., Godos, J., Galvano, F., & Giovannucci, E. L. (2017). Coffee, caffeine, and health outcomes: an umbrella review. *Annual review of nutrition*, *37*, 131-156.

Hernán, M. A., Takkouche, B., Caamaño-Isorna, F., & Gestal-Otero, J. J. (2002). A meta-analysis of coffee drinking, cigarette smoking, and the risk of Parkinson's disease. *Annals of neurology*, *52*(3), 276-284.

Chen, H., Zhang, S. M., Schwarzschild, M. A., Hernan, M. A., & Ascherio, A. (2005). Physical activity and the risk of Parkinson disease. *Neurology*, *64*(4), 664-669.

Karimi-Moghadam A, Charsouei S, Bell B, Jabalameli MR. Parkinson Disease from Mendelian Forms to Genetic Susceptibility: New Molecular Insights into the Neurodegeneration Process. Cell Mol Neurobiol. 2018 Aug;38(6):1153-1178. doi: 10.1007/s10571-018-0587-4. Epub 2018 Apr 26. PMID: 29700661; PMCID: PMC6061130.

Mike A Nalls, Cornelis Blauwendraat, and et al. Identification of novel risk loci, causal insights, and heritable risk for parkinson’s disease: a meta-analysis of genome-wide association studies. The Lancet Neurology, 18:1091–1102, 12

Corti, O., Lesage, S., & Brice, A. (2011). What genetics tells us about the causes and mechanisms of Parkinson's disease. *Physiological reviews*.

Zhang, L. I., Shimoji, M., Thomas, B., Moore, D. J., Yu, S. W., Marupudi, N. I., ... & Dawson, V. L. (2005). Mitochondrial localization of the Parkinson's disease related protein DJ-1: implications for pathogenesis. *Human molecular genetics*, *14*(14), 2063-2073.

Iannotta, L., & Greggio, E. (2021). LRRK2 signaling in neurodegeneration: two decades of progress. *Essays in Biochemistry*, *65*(7), 859-872.

Wallings, R. L., & Tansey, M. G. (2019). LRRK2 regulation of immune-pathways and inflammatory disease. *Biochemical Society Transactions*, *47*(6), 1581-1595.

Russo, I., Berti, G., Plotegher, N., Bernardo, G., Filograna, R., Bubacco, L., & Greggio, E. (2015). Leucine-rich repeat kinase 2 positively regulates inflammation and down-regulates NF-κB p50 signaling in cultured microglia cells. *Journal of neuroinflammation*, *12*(1), 1-13.

Usmani, A., Shavarebi, F., & Hiniker, A. (2021). The cell biology of LRRK2 in Parkinson's disease. *Molecular and Cellular Biology*, *41*(5), e00660-20.

Cogo, S., Manzoni, C., Lewis, P. A., & Greggio, E. (2020). Leucine-rich repeat kinase 2 and lysosomal dyshomeostasis in Parkinson disease. *Journal of neurochemistry*, *152*(3), 273-283.

Ho, D. H., Lee, H., Son, I., & Seol, W. (2019). G2019s LRRK2 promotes mitochondrial fission and increases TNFα-mediated neuroinflammation responses. *Animal Cells and Systems*, *23*(2), 106-111.

Weindel, C. G., Bell, S. L., Vail, K. J., West, K. O., Patrick, K. L., & Watson, R. O. (2020). LRRK2 maintains mitochondrial homeostasis and regulates innate immune responses to Mycobacterium tuberculosis. *Elife*, *9*, e51071.

Bonet-Ponce, L., & Cookson, M. R. (2022). LRRK2 recruitment, activity, and function in organelles. *The FEBS Journal*, *289*(22), 6871-6890.

Zhang, M., Li, C., Ren, J., Wang, H., Yi, F., Wu, J., & Tang, Y. (2022). The double-faceted role of leucine-rich repeat kinase 2 in the immunopathogenesis of Parkinson’s disease. *Frontiers in Aging Neuroscience*, *14*, 909303.

Pfeffer, S. R. (2023). LRRK2 phosphorylation of Rab GTPases in Parkinson's disease. *FEBS letters*, *597*(6), 811-818.

Pickrell, A. M., & Youle, R. J. (2015). The roles of PINK1, parkin, and mitochondrial fidelity in Parkinson’s disease. *Neuron*, *85*(2), 257-273.

Narendra, D. P., Jin, S. M., Tanaka, A., Suen, D. F., Gautier, C. A., Shen, J., ... & Youle, R. J. (2010). PINK1 is selectively stabilized on impaired mitochondria to activate Parkin. *PLoS biology*, *8*(1), e1000298.

Seok Min Jin and Richard J. Youle. Pink1-and parkin-mediated mitophagy at a glance. Journal of Cell Science, 125:795–799, 2 2012.

Sellgren, C., Sheridan, S., Gracias, J. *et al.* Patient-specific models of microglia-mediated engulfment of synapses and neural progenitors. *Mol Psychiatry* **22**, 170–177 (2017).

Rio-Hortega, P. D. (1920). Estudios sobre la neuroglía. La microglía y su transformación en células en bastoncito y cuerpos granuloadiposos. *Trab. Lab. Invest. Biol. Univ. Madrid*, *18*, 37-82.

Ungvari, Z., Krasnikov, B. F., Csiszar, A., Labinskyy, N., Mukhopadhyay, P., Pacher, P., ... & Podlutsky, A. (2008). Testing hypotheses of aging in long-lived mice of the genus Peromyscus: association between longevity and mitochondrial stress resistance, ROS detoxification pathways, and DNA repair efficiency. *Age*, *30*, 121-133.

Bussian, T. J., Aziz, A., Meyer, C. F., Swenson, B. L., van Deursen, J. M., & Baker, D. J. (2018). Clearance of senescent glial cells prevents tau-dependent pathology and cognitive decline. *Nature*, *562*(7728), 578-582.

Guneykaya, D., Ivanov, A., Hernandez, D. P., Haage, V., Wojtas, B., Meyer, N., ... & Wolf, S. A. (2018). Transcriptional and translational differences of microglia from male and female brains. *Cell reports*, *24*(10), 2773-2783.

Villa, A., Gelosa, P., Castiglioni, L., Cimino, M., Rizzi, N., Pepe, G., ... & Maggi, A. (2018). Sex-specific features of microglia from adult mice. *Cell reports*, *23*(12), 3501-3511.

Mazzolini, J., Le Clerc, S., Morisse, G., Coulonges, C., Kuil, L. E., Van Ham, T. J., ... & Sieger, D. (2020). Gene expression profiling reveals a conserved microglia signature in larval zebrafish. *Glia*, *68*(2), 298-315.

Hammond, T. R., Dufort, C., Dissing-Olesen, L., Giera, S., Young, A., Wysoker, A., ... & Stevens, B. (2019). Single-cell RNA sequencing of microglia throughout the mouse lifespan and in the injured brain reveals complex cell-state changes. *Immunity*, *50*(1), 253-271.

Li, Q., Cheng, Z., Zhou, L., Darmanis, S., Neff, N. F., Okamoto, J., ... & Barres, B. A. (2019). Developmental heterogeneity of microglia and brain myeloid cells revealed by deep single-cell RNA sequencing. *Neuron*, *101*(2), 207-223.

Bryan, N. B., Dorfleutner, A., Rojanasakul, Y., & Stehlik, C. (2009). Activation of inflammasomes requires intracellular redistribution of the apoptotic speck-like protein containing a caspase recruitment domain. *The Journal of Immunology*, *182*(5), 3173-3182.

Janks, L., Sharma, C.V.R. & Egan, T.M. A central role for P2X7 receptors in human microglia. *J Neuroinflammation* 15, 325 (2018).

Rampe D, Wang L, Ringheim GE. P2X7 receptor modulation of beta-amyloid- and LPS-induced cytokine secretion from human macrophages and microglia. J Neuroimmunol. 2004 Feb;147(1-2):56-61.

Francistiová L, Vörös K, Lovász Z, Dinnyés A, Kobolák J. Detection and Functional Evaluation of the P2X7 Receptor in hiPSC Derived Neurons and Microglia-Like Cells. Front Mol Neurosci. 2022 Jan 12;14:793769.

Saijo, K., Glass, C. Microglial cell origin and phenotypes in health and disease. *Nat Rev Immunol* 11, 775–787 (2011).

Mouton-Liger, F., Rosazza, T., Sepulveda-Diaz, J., Ieang, A., Hassoun, S. M., Claire, E., ... & Corti, O. (2018). P arkin deficiency modulates NLRP 3 inflammasome activation by attenuating an A 20-dependent negative feedback loop. *Glia*, *66*(8), 1736-1751.

Tolosa, E., Vila, M., Klein, C., & Rascol, O. (2020). LRRK2 in Parkinson disease: challenges of clinical trials. *Nature Reviews Neurology*, *16*(2), 97-107.

Atashrazm, F., & Dzamko, N. (2016). LRRK2 inhibitors and their potential in the treatment of Parkinson's disease: current perspectives. *Clinical pharmacology: advances and applications*, 177-189.

Hu, J., Zhang, D., Tian, K., Ren, C., Li, H., Lin, C., ... & Zhang, J. (2023). Small-molecule LRRK2 inhibitors for PD therapy: Current achievements and future perspectives. *European Journal of Medicinal Chemistry*, 115475.

Jennings, D., Huntwork-Rodriguez, S., Vissers, M. F., Daryani, V. M., Diaz, D., Goo, M. S., ... & Troyer, M. D. (2023). LRRK2 inhibition by BIIB122 in healthy participants and patients with Parkinson's disease. *Movement Disorders*, *38*(3), 386-398.

Sargeant, T. J., & Fourrier, C. (2022). Human monocyte-derived microglia-like cell models: A review of the benefits, limitations and recommendations. *Brain, Behavior, and Immunity*.

Gosselin, D., Skola, D., Coufal, N. G., Holtman, I. R., Schlachetzki, J. C., Sajti, E., ... & Glass, C. K. (2017). An environment-dependent transcriptional network specifies human microglia identity. *Science*, *356*(6344), eaal3222.

Ryan, K. J., White, C. C., Patel, K., Xu, J., Olah, M., Replogle, J. M., ... & Bradshaw, E. M. (2017). A human microglia-like cellular model for assessing the effects of neurodegenerative disease gene variants. *Science translational medicine*, *9*(421), eaai7635.

Banerjee, A., Lu, Y., Do, K., Mize, T., Wu, X., Chen, X., & Chen, J. (2021). Validation of induced microglia-like cells (iMG Cells) for future studies of brain diseases. *Frontiers in Cellular Neuroscience*, *15*, 629279.

ROCHET, Jean-Christophe, FLEMING OUTEIRO, Tiago, CONWAY, Kelly A., *et al.* Interactions among α-synuclein, dopamine, and biomembranes: some clues for understanding neurodegeneration in Parkinson's disease. *Journal of Molecular Neuroscience*, 2004, vol. 23, p. 23-33.

Jackson-Lewis, V., Smeyne, R.J. MPTP and SNpc DA neuronal vulnerability: Role of dopamine, superoxide and nitric oxide in neurotoxicity. Minireview.. *neurotox res* **7**, 193–201 (2005).

Shapira, A. H. V. et al. Anatomic and disease specificity of NADH CoQ, reductase (complex I) deficiency in Parkinson's disease. *J. Neurochem.* **55**, 2142–2145 (1990)

Elbaz, A., Carcaillon, L., Kab, S., & Moisan, F. (2016). Epidemiology of Parkinson's disease. *Revue neurologique*, *172*(1), 14-26.